

Impacts of a Pinatubo-Size Volcanic Eruption on ENSO

Evgeniya Predybaylo,¹ Georgiy L. Stenchikov,¹ Andrew T. Wittenberg,²

Fanrong Zeng²

Evgeniya Predybaylo, evgeniya.predybaylo@kaust.edu.sa

¹King Abdullah University of Science and
Technology, Thuwal, Saudi Arabia.

²NOAA Geophysical Fluid Dynamics
Laboratory, Princeton, USA

This article has been accepted for publication and undergone full peer review but has not been through the copyediting, typesetting, pagination and proofreading process, which may lead to differences between this version and the Version of Record. Please cite this article as doi: 10.1002/2016JD025796

Abstract.

Observations and model simulations of the climate responses to strong explosive low-latitude volcanic eruptions suggest a significant increase in the likelihood of El Niño during the eruption and post-eruption years, though model results have been inconclusive and have varied in magnitude and even sign. In this study, we test how this spread of responses depends on the initial phase of El Niño-Southern Oscillation (ENSO) in the eruption year, and on the eruption's seasonal timing. We employ the GFDL CM2.1 global coupled general circulation model to investigate the impact of the Pinatubo 1991 eruption, assuming that in 1991 ENSO would otherwise be in Central or Eastern Pacific El Niño, La Niña, or neutral phases. We obtain statistically significant El Niño responses in a year after the eruption for all cases except La Niña, which shows no response in the eastern equatorial Pacific. The eruption has a weaker impact on Eastern Pacific El Niños than on Central Pacific El Niños. We find that the ocean dynamical thermostat, and (to a lesser extent) wind changes due to land-ocean temperature gradients, are the main feedbacks affecting El Niño development after the eruption. The El Niño responses to eruptions occurring in summer are more pronounced than for winter and spring eruptions. That the climate response depends on eruption season and initial ENSO phase may help to reconcile apparent inconsistencies among previous studies.

Keypoints:

- In our simulations the likelihood of El Niño-like responses almost doubles after a Pinatubo-size eruption
- The Central Pacific El Niños develop much stronger warming responses to volcanic forcing than the Eastern Pacific El Niños
- El Niño responses are highly sensitive to the seasonal timing of a Pinatubo-size eruption

1. Introduction

Volcanic radiative impacts are important climate drivers on multiple time scales [Robock, 2000; Stenchikov, 2009; Timmreck, 2012; Meehl *et al.*, 2015; Timmreck *et al.*, 2016]. Large explosive volcanic eruptions inject sulfur-rich gases into the stratosphere [Newhall and Self, 1982; Schnetzler *et al.*, 1997], where they get converted into sulfate aerosols [Turco *et al.*, 1983; Lamb, 1970; LeGrande *et al.*, 2016]. These aerosols scatter light in ultraviolet and visible spectra, absorb and scatter in the near-infrared, and absorb, scatter, and emit thermal longwave radiation [Lacis *et al.*, 1992; Hansen *et al.*, 1997; Stenchikov *et al.*, 1998], affecting the energy balance of the planet. As a result, the global mean surface temperature cools, and the lower stratosphere heats up [Minnis *et al.*, 1993; Stenchikov *et al.*, 1998; Rind and Lacis, 1993; Turco *et al.*, 1983; De Silva and Zielinski, 1998; Briffa *et al.*, 1998; Santer *et al.*, 2014]. The associated redistribution of radiative heating directly impacts atmospheric circulation [Rind *et al.*, 1992; Stenchikov *et al.*, 2006] and cools the ocean [Church *et al.*, 2005; Gleckler *et al.*, 2006; Stenchikov *et al.*, 2009; Otterå *et al.*, 2010], producing global and regional changes in the Earth's climate system [Otterå *et al.*, 2010; Fischer *et al.*, 2007; Haywood *et al.*, 2013] and affecting the major modes of climate variability. Impacts of volcanic eruptions on the North Atlantic/Arctic oscillation have been a subject of active research over the past 15-20 years [Robock and Mao, 1995; Stenchikov *et al.*, 2002, 2006].

The El Niño-Southern Oscillation (ENSO) is one of the most important climate variability modes, which controls the climate not only in the equatorial Pacific [Soden, 2000] but also impacts the entire globe [Brönnimann *et al.*, 2007; Ineson and Scaife, 2009; Graf

and Zanchettin, 2012]. It perturbs the hydrological cycle [Soden, 2000], multidecadal biological and bio-geochemical cycles of the ocean [Chavez *et al.*, 2003; Yoder and Kennelly, 2003], and affects hurricane [Goldenberg *et al.*, 2001; Gray, 1984; Vecchi *et al.*, 2014] and tornado [Lee *et al.*, 2016] activity and precipitation patterns [Ropelewski and Halpert, 1987, 1996; Ratnam *et al.*, 2014; Jia *et al.*, 2015]. ENSO causes an anomalous change in the air-sea interaction in the equatorial Pacific every 2-7 years [Trenberth, 1997; D'Arrigo *et al.*, 2005]. The positive (El Niño) and negative (La Niña) phases are asymmetric in magnitude, and have different spatial-temporal appearance and intensity [Choi *et al.*, 2013, 2015]. Generally, El Niños have a strong stochastic component associated with westerly wind bursts (WWBs), while La Niñas are more likely to occur immediately after strong El Niños. For this reason, it is usually easier to predict La Niñas than El Niños. Although predictions and projections of ENSO remain a challenge due to the strong non-linearity of ENSO processes and their high sensitivity to external forcing [Wittenberg, 2002; Collins *et al.*, 2010; DiNezio *et al.*, 2012; Watanabe *et al.*, 2012; Choi *et al.*, 2013; Lee *et al.*, 2014; Wittenberg *et al.*, 2014], accurate future projections of ENSO behavior are crucial to assess future climate risks [Vecchi and Wittenberg, 2010; Capotondi *et al.*, 2015; Wittenberg, 2015; Guilyardi *et al.*, 2016], and for societal decision-making [Cash *et al.*, 2006].

Most of the largest eruptions of the 20th century occurred in El Niño years - e.g., El Chichón in April 1982, and Pinatubo in June 1991 (Figure 1). It was confirmed recently that the Tambora eruption, which produced about three times more sulfur dioxide than Pinatubo and caused the “Year without a summer” in 1816, was also accompanied by an El Niño [Raible *et al.*, 2016]. The nature of these relationships is not well understood,

but they have dramatic consequences for the entire planet – thus it is important to better investigate the mechanism of volcanic impacts on ENSO [*Stenchikov*, 2009; *Li et al.*, 2011; *Timmreck*, 2012; *Wittenberg et al.*, 2014], which could explain some of its temporal modulation in historical and paleo records, and their relation to internal ENSO dynamics [*Emile-Geay et al.*, 2008; *Vecchi and Wittenberg*, 2010; *Emile-Geay et al.*, 2013; *McGregor et al.*, 2013; *Ogata et al.*, 2013; *Atwood et al.*, 2016].

Given the brevity of in situ and satellite observational records, the actual volcanic forcing impact on ENSO cannot easily be empirically determined. Studies based on paleo data [*Adams et al.*, 2003; *McGregor et al.*, 2010; *Wahl et al.*, 2014; *Li et al.*, 2013] detected a remarkable shift in tropical Pacific climate in post-volcanic years towards an El Niño-like state or a multi-year El Niño. The direct effect of volcanic forcing cools the surface; e.g. *Li et al.* [2013] emphasized the importance of tropical Pacific sea surface temperature (SST) cooling shortly after the eruption. This cooling takes place prior to the development of an extra El Niño-like warming the year after an eruption. The physical interpretation of the initial cooling is still under question. *McGregor and Timmermann* [2011] captured this phenomenon using the Community Climate System Model (CCSM3), however, in their study the amplitude of simulated cooling was overestimated, and the subsequent warming was quantitatively inconsistent with temperatures inferred from proxy records.

In one of the first modeling studies on volcanic impacts on ENSO, *Hirono* [1988] suggested that absorption of solar and terrestrial radiation by volcanic aerosols led to atmospheric heating, which produced a wind anomaly that triggered an El Niño event. This interaction was further studied by *Robock et al.* [1995] with the help of an atmospheric general circulation model (GCM) NCAR CCM1. *Robock et al.* [1995] calculated the effect

of the El Chichón eruption and concluded that at the time of the eruption, the El Niño in the Spring of 1982 was already underway, so it was not caused by the eruption; however, volcanic forcing might have affected the El Niño amplitude.

Mann et al. [2005] and *Emile-Geay et al.* [2008] studied volcanic impacts on ENSO, using the simplified coupled atmosphere-ocean model of *Zebiak and Cane* [1987]. *Emile-Geay et al.* [2008] performed large ensemble experiments testing the tropical Pacific response to strong volcanic forcing. They found that only very powerful eruptions of more than an order of magnitude stronger than Pinatubo could lead to a correlation between volcanic forcing and El Niño and therefore affect El Niño likelihood and/or magnitude. The simplicity of the Cane-Zebiak model precluded a reliable quantitative determination of the level of volcanic forcing needed for an ENSO response, leaving uncertain whether Pinatubo was above or below this threshold. Both papers, however, suggested that strong volcanic forcing affects ENSO and tropical Pacific climate via the ocean dynamical thermostat (ODT) mechanism [*Seager et al.*, 1988; *Clement et al.*, 1996], in which surface perturbations are displaced by upwelling of deeper, unperturbed waters.

Ohba et al. [2013] confirmed the findings of *Adams et al.* [2003] and *McGregor et al.* [2010] using an interim version of the Model for Interdisciplinary Research on Climate (MIROC) [*Watanabe et al.*, 2010]. They investigated the sensitivity of ENSO to volcanic forcings of realistic strength (1.5 x Pinatubo, and 0.5, 1.5 and 2 scaling of that value) as well as the background ENSO phase: neutral, positive and negative. They suggested that the ODT is not the sole mechanism affecting the SST response; there is also a strong contribution of the atmospheric response to the changes in the land-ocean temperature gradient in the Western Pacific (WP).

Maher et al. [2015] analysed the tropical Pacific climate state in the composite CMIP3 and CMIP5 historical simulations after the five strongest eruptions. They also found a tendency toward an El Niño-like (La Niña-like) SST response in the first (third) year after an eruption. However, only a third of the examined models were able to simulate a realistic ENSO [*Kim et al.*, 2014; *Kim and Jin*, 2011].

The most recent studies on the topic [*Pausata et al.*, 2015; *Lim et al.*, 2015; *Stevenson et al.*, 2016] discussed a shift of the Intertropical Convergence Zone (ITCZ) as an alternative mechanism of volcano-El Niño interaction, induced by a very strong (more than 15 W m^{-2}) radiative forcing that is asymmetric with respect to the equator. *Stevenson et al.* [2017] used the Community Earth System Model (CESM) to study responses to volcanic eruptions occurred in January, April, July, and October, calculating aerosol distributions interactively within the model. They found a cooling response during the first six months after an eruption, which they interpreted as resulting from reduced downward shortwave flux (especially in the relatively cloud-clear east Pacific) which strengthened the zonal SST gradient along the equator, and shifted the ITCZ northward. The initial La Niña-like cooling in the CESM was then followed by an El Niño-like warming of the east Pacific, which *Stevenson et al.* [2017] suggested being caused by an induced off-equatorial anticyclonic wind stress curl that forced an equatorward Sverdrup transport of heat in the upper ocean.

Thus, the sensitivity studies conducted so far [*Mann et al.*, 2005; *Emile-Geay et al.*, 2008; *McGregor and Timmermann*, 2011; *Ohba et al.*, 2013; *Lim et al.*, 2015; *Stevenson et al.*, 2017] reveal that simulation results are model dependent, and do not fully illuminate the mechanisms of volcanic impacts on ENSO.

Many studies [Ashok *et al.*, 2007; Kug *et al.*, 2010; Lee *et al.*, 2014; Chen *et al.*, 2015; Capotondi *et al.*, 2015; Chen *et al.*, 2016] have highlighted the diversity of ENSO events, mechanisms, and impacts. The Pinatubo eruption coincided with a moderate Central Pacific (CP) El Niño that lasted for about two years [Kessler and McPhaden, 1995], and the eruption of El Chichón was accompanied by a very strong Eastern Pacific (EP) El Niño that behaved differently from that in the Pinatubo case. Here we hypothesize that the initial ENSO state, including the different El Niño types, may play a key role in the diverse tropical Pacific responses to volcanic eruptions. We focus on the following questions:

1. What causes the diversity of ENSO responses to Pinatubo-size volcanic forcing in observations and model simulations?
2. What atmospheric and oceanic feedbacks tend to amplify or damp the ENSO response?
3. How do ENSO responses and feedbacks depend on the preconditioning of the tropical Pacific climate system?
4. How sensitive is ENSO to small perturbations, and how different might ENSO responses be to volcanic eruptions occurring at different times of year?

2. Methodology

To answer the above questions, we employ a global coupled ocean-atmosphere GCM, CM2.1, developed by the Geophysical Fluid Dynamics Laboratory (GFDL) [Delworth *et al.*, 2006], which was used for the Coupled Model Intercomparison Project phase 3 (CMIP3) and the IPCC Fourth Assessment Report (IPCC AR4), as well as in our previous

studies on the volcanic impact on atmospheric and oceanic circulations involving the Arctic Oscillation and Atlantic Meridional Overturning Circulation [*Stenchikov et al.*, 2006; *Stenchikov*, 2009; *Stenchikov et al.*, 2009].

2.1. Model Description

Here we briefly summarize the formulation of the CM2.1 global coupled GCM. Its atmospheric component [*Anderson et al.*, 2004] has a horizontal grid spacing of 2° latitude by 2.5° longitude, with 24 vertical levels and a finite volume dynamical core [*Lin*, 2004]. The land surface component [*Milly and Shmakin*, 2002] has the same horizontal resolution as the atmospheric component. The ocean component [*Griffies et al.*, 2005; *Gnanadesikan et al.*, 2006] is implemented on a tripolar horizontal grid, with zonal spacing of 1° , and meridional spacing telescoping from 1° at high latitudes to $1/3^\circ$ near the equator. The ocean model has 50 vertical levels, with 10 m spacing over the top 220 m. The ocean and atmosphere are coupled every 2 hours. The atmospheric composition, incoming solar radiation, and land cover are kept at the 1990 level.

CM2.1's tropical Pacific and ENSO simulation characteristics have been extensively discussed [e.g. *Wittenberg et al.*, 2006; *Wittenberg*, 2009; *Kug et al.*, 2010; *Wittenberg et al.*, 2014; *Karamperidou et al.*, 2014; *Atwood et al.*, 2016; *Chen et al.*, 2016]. While the simulated SST, winds, surface fluxes and oceanic subsurface temperature do have biases in some regions, they generally agree well with observations. *Wittenberg et al.* [2006] and *Wittenberg* [2009] showed that CM2.1 captures the main aspects of tropical Pacific climate and ENSO. In addition, *Kim and Jin* [2011] showed that CM2.1 is one of the few models able to produce a stable, realistic ENSO under various external forcing perturbations.

Kug et al. [2010] and *Capotondi et al.* [2015] discussed CM2.1's ability to successfully reproduce realistic CP and EP El Niño patterns and frequencies (Table 1).

2.2. Experimental Setup

Generally, ENSO comprises El Niño, La Niña and neutral phases. However, El Niños can be of multiple types that can be split roughly into CP and EP groups [*Ashok et al.*, 2007; *Kug et al.*, 2010; *Lee et al.*, 2014; *Chen et al.*, 2015; *Capotondi et al.*, 2015; *Chen et al.*, 2016]. CP and EP El Niño types are characterized by a distinct genesis. Observations show that weak and moderate El Niños mostly tend to be of the CP type, while the strong El Niños usually follow a canonical EP pattern [*Rasmusson and Carpenter*, 1982; *Zheng et al.*, 2014; *Fang et al.*, 2015]. *Kug et al.* [2010] showed that the formation of the moderate El Niño is the product of zonal advection, while the strong El Niño involves a greater role for vertical advection. *Chen et al.* [2015] argued that chaotically generated WWBs play a key role in El Niño formation. WWBs occur sporadically during November (in the year before the event)-May (in the year of the event) and strongly impact ENSO variability [*Vecchi et al.*, 2006]. WWBs have been shown to play a role in triggering and amplifying El Niño [*Gebbie et al.*, 2007; *Zavala-Garay et al.*, 2008; *Wittenberg et al.*, 2014; *Atwood et al.*, 2016], as well as affecting its type [*Chen et al.*, 2015].

The development of a moderate El Niño is initiated by WWBs that cause eastward advection of warm water towards the CP. Consequently, the SST gradient between the WP and CP decreases, and results in a reduction of the easterly trade winds over the WP. This causes CP SST warming via the Bjerknes feedback mechanism [*Bjerknes*, 1969] and further decreases the SST gradient. The resultant CP El Niño onset slightly reduces the EP upwelling, but does not shut it down completely, allowing the EP to remain cold.

Strong WWBs frequently serve as forerunners of extremely strong El Niño events, by driving the multiple oceanic Kelvin wave pulses that accumulate warm water in the EP. Thus, an expanded warm pool develops early in September-October of an El Niño year, and SST anomalies peak in the boreal winter near the eastern boundary, almost completely shutting down the equatorial upwelling. The related equatorial Pacific westerly wind anomaly is greater for EP than CP El Niños, due to a stronger response of the zonal surface pressure gradient. CM2.1 generally captures all these features, though *Wittenberg et al.* [2006] noted that in CM2.1 westerly wind anomalies formed due to the Bjerknes effect are located further west than in the real world.

In our simulations, we examine the impact of Pinatubo forcing on different El Niños, which tend to peak around December of 1991, coinciding with the peak in the Pinatubo volcanic forcing that develops half a year after the eruption. Below we refer to 1991 as the initial year of the simulation or the year of eruption, and 1992 and 1993 as the first and second years after the eruption, respectively.

Having noted the above differences in amplitude, spatial pattern and genesis of the CP and EP El Niños, it is important to study the different ways in which EP and CP El Niños respond to an eruption. We consider a complete set of initial conditions (ICs) to cover the possible initial ENSO phases that could occur in the year of an eruption. We do not suggest a causal relationship between volcanic eruptions and ENSO at the time of eruption; instead, we assume that the eruption could happen in either neutral ENSO, El Niño (CP or EP), or La Niña conditions, which occur with different probabilities (see Table 1). We then examine the evolution of the volcanically perturbed ENSO probability distribution, relative to that of unperturbed or infinitesimally perturbed simulations.

In order to simulate the volcanic perturbation, we prescribe the Pinatubo aerosols' optical properties according to *Stenchikov et al.* [2006, 2009] using optical depth from *Sato et al.* [1993]. This volcanic dataset provides zonally averaged monthly mean spectral dependent aerosol extinction, single scattering albedo, and an asymmetry parameter which are required to conduct radiative transfer simulations within CM2.1. The experimental design allows the corresponding ENSO conditions to freely develop before the eruption, exactly as in the present-day control run, and then the Pinatubo forcing is applied in June 1991. The control and perturbed runs first diverge in mid-May 1991, because the monthly mean aerosol characteristics are interpolated between the months.

We conducted four 10-member ensemble integrations of control (CTR, without volcanic aerosols) and perturbed (PRT, with volcanic aerosols) experiments with ENSO-neutral, La Niña, CP El Niño, and EP El Niño occurring in the initial year of each control experiment (see Table 2). The ensemble of 10 different ICs from each ENSO category is intended to capture the intrinsic variability of the climate system. To increase the signal-to-noise ratio, we present our results using ensemble means, and use the ensemble spread to calculate statistical significance. We implement three methods of calculating anomalies. Based on the climatology (CLM) computed from the present-day control run conducted by *Delworth et al.* [2006], using monthly averages over years 101–200 of the 300-year simulation, we calculate the control and perturbed anomalies by subtracting the climatology from the control and perturbed runs, respectively. CTR-CLM represents a pure ENSO signal, and the difference PRT-CTR (which we call the “response”) shows the ENSO response to volcanic forcing, as the “control ENSO” effect is removed. Statistical significance of the

ensemble mean differences is computed using a two-tailed Student's t-test at the 0.05 significance level.

We start each ensemble simulation from January 1, 1991 with the coupled atmosphere-ocean IC extracted from the 300-year present-day control run. The ENSOs present in this run were categorized by their strength and associated spatial pattern according to the threshold values of the boreal winter (October/November/December - OND) NINO3.4 index. The chosen ENSOs are then combined into 10-member control ensembles of ENSO-neutral (with OND Niño3.4 < 0.15 K), weak/CP El Niño (with OND Niño3.4 index range 1.4 - 1.8 K), strong/EP El Niño (with OND Niño3.4 index range 3.4 - 4.7 K), and La Niña (with OND NINO3.4 < -1 K) named *NTE*, *CPE*, *EPE*, and *LAN* ensembles, respectively.

Figure 2 shows control 10-member ensemble mean surface temperature anomalies, wind stress anomalies, and total precipitation, in December of 1991 for all experiments.

2.3. Observational Data

For calculations of the observed Niño 3.4 index (Figure 1), we use monthly mean SSTs from the NOAA Extended Reconstructed SST (ERSST) V4 dataset [Huang *et al.*, 2015]. The data have a spatial resolution of 2° latitude by 2° longitude, and cover January 1854-present. The climatology is computed as monthly averages from the data for years 1880-2000. Figure 1 shows that the Niño 3.4 SST anomaly trajectories following the El Chichón (1982) and Pinatubo (1991) eruptions evolve quite differently. The El Niño of 1982 is stronger than that of 1991, but terminates sooner. The 1982 El Niño is followed by a prolonged La Niña, while the weaker and longer El Niño of 1991 is followed by prolonged El Niño warm anomalies.

The observed ENSO frequencies (Table 1) are calculated using the ERSST V4 dataset for the period 1980-2010. CP El Niño events are identified following *Pascolini-Campbell et al.* [2015] method based on combination of nine different SST-based indices (see Table 1 in *Pascolini-Campbell et al.* [2015]) complemented by the visual examination of spatial patterns.

3. Results

Imposing the prescribed volcanic aerosols in the model results in a reduction of the shortwave (SW) radiation reaching the surface. The longwave (LW) effect of volcanic aerosols at the surface is relatively small and insignificant [*Stenchikov et al.*, 1998]. Figure 3 represents the time evolution of the 10-member ensemble mean (PRT-CTR) all-sky net (down - up) surface SW radiative flux response, averaged globally and over the tropical belt (20°S-20°N) for *NTE*, *CPE*, *EPE* and *LAN* ensembles. The net SW radiative surface response in the tropics peaks at -5.5 W m^{-2} in the fall of 1991, as the SO_2 mass conversion *e*-folding time is about 35 days, and the aerosol layer fully develops by then [*Stenchikov et al.*, 1998]. The global net SW radiative surface response of -3 W m^{-2} peaks six months after the eruption, because of the interaction of conversion and transport processes. In the *CPE* and *EPE* experiments, we see weaker forcing in the winter of 1991, due to El Niño-induced increases in cloud cover. The volcanic radiative effect is present for more than two years, and is quite similar in the different ensembles — apart from incoherent chaotic fluctuations among the different cases, which are not completely removed by the 10-member ensemble mean.

Figure 4 depicts the global and tropical mean surface temperature responses (PRT-CTR) to volcanic forcing. Half a year after the eruption the surface temperature decreases

by about 0.4 K globally, which is in a good agreement with observations and other modeling studies [Dutton and Christy, 1992; Hansen *et al.*, 1992; McCormick *et al.*, 1995; Soden *et al.*, 2002]. The surface temperature relaxes slowly because of the high thermal capacity of the ocean. According to Stenchikov *et al.* [2009] it takes about a decade for the atmosphere and upper ocean system to equilibrate (not shown). In the tropics, the surface temperature fluctuations are higher and depend on the initial ocean state, demonstrating warmer anomalies in comparison with the global ones in the *NTE* and *CPE* cases during 1992 and beginning of 1993.

Figure 5 shows the 10-member ensemble mean perturbations of the Niño 3.4 SST. Red curves show the isolated effect of volcanic forcing on ENSO. The Pinatubo volcanic forcing causes a statistically significant increase of the Niño 3.4 index in summer 1992 in the *NTE* and *CPE* ensembles. The *NTE* ensemble transforms into a moderate-to-weak El Niño-like warming in the second winter after the eruption that lasts more than a year (Figure 5a); and in the *CPE* 10-member ensemble mean, El Niño extends for an extra year (Figure 5b). Distinctively, in the *EPE* ensemble the El Niño weakens in winter of 1991, and is followed by less of a prolongation of El Niño than in the *NTE* and *CPE* cases (Figure 5c). The *LAN* ensemble does not show any notable changes (Figure 5d), and for this reason we do not show the *LAN* responses further.

3.1. Volcanic impacts at different ENSO phases

Figure 6 displays Hovmöller diagrams of SST, zonal wind, net surface heat flux, all-sky net (down-up) shortwave flux at the surface, latent heat flux, and total cloud amount responses (PRT-CTR) for the *NTE*, *CPE*, and *EPE* ensembles. Shortly after the eruption, the equatorial Pacific region is subject to a strong SW radiation reduction (Figure

6a,i,q). The uniformly distributed clear-sky radiative forcing is modulated by clouds. All-sky radiative forcing drives climate changes and could itself cause about 0.3 K global SST cooling [Stenchikov *et al.*, 2009].

The land initially cools faster than the ocean, and the associated land-ocean temperature gradient (LOTG) both in the WP and EP generates zonal wind anomalies, which, in turn, affect ocean temperature in the initial stage of the process [Ohba *et al.*, 2013]. The ocean dynamical thermostat (ODT) mechanism [Seager *et al.*, 1988; Clement *et al.*, 1996] comes into play later, as the ocean responds more slowly to the radiative forcing. The ODT mechanism triggers non-uniform SST changes in the equatorial Pacific due to a differential ocean response to the spatially uniform radiative forcing. The efficiency and duration of these mechanisms depend on the background ocean state, therefore ENSO responses appear to be different for different ICs (Figure 5).

3.1.1. *NTE* ensemble

Figure 6b shows that in the *NTE* case during the first three months after the eruption, the LOTG (PRT-CTR) response in the WP is stronger than in the EP, because the EP ocean surface and nearby land areas in the background state are cold (Figure 2a). The developed WP LOTG decreases the trade winds in the WP (Figure 6c) west of 140°E. This westerly wind anomaly allows more warm water to advect eastward and favors WWBs. Both effects (enhanced westerlies and WWBs) are usually important forerunners of an El Niño event. However, because of the land's low thermal capacity, this LOTG mechanism is short-lived and lasts for 2-3 months until the ocean temperature adjusts to the radiative forcing.

The SST changes are further supported by the ODT mechanism. Specifically, in Figure 6b we see a significant WP SST reduction starting in October of 1991, while the EP SST remains unperturbed. Such a spatially varying response of the ocean surface to a uniform atmospheric forcing is due to the upwelling which is strong in the CP and EP and regulates the SST there. Cooling of the WP SST increases sea level pressure (SLP, not shown) in the WP, enhances CP westerly wind anomalies, and results in a further reduction of the easterly trade winds (Figure 6c). This activates the Bjerknes feedback [Bjerknes, 1969] and leads to a positive SST anomaly in the EP (Figure 6b). It is important to note that the relatively weak El Niño-like SST response in the *NTE* case does not completely shut down the upwelling (Figure 2a), and therefore the ODT mechanism is functioning throughout the period of volcanic forcing. Although the wind feedback is controlled by the ODT mechanism, it is also intensified by the eastward shift of the deep convection (Figure 6g), which tends to follow the warmest SSTs as explained in detail in Choi *et al.* [2015].

To evaluate the effect of the surface energy balance change we calculate the net energy flux $NF = SW + LW + SH + LH$, where SW is the net (down-up) shortwave flux, LW is the net (down-up) longwave flux, SH is the sensible heat flux, and LH is the latent heat flux at the surface. The net surface heat flux response is negative in the areas with a positive SST response, thus tending to damp the latter. Figure 6d,e,f shows that the all-sky surface radiative and LH fluxes in the first and second years after the eruption mostly damp the SST response. The main contributors to the net energy flux anomaly are the SW and LH fluxes (see Figure 6e,f). The presence of clouds in the tropical Pacific changes the distribution of the incoming solar radiation: the all-sky SW response is negative over

the warmer ocean areas, as the warmer ocean favors more shading by convective clouds. Similarly, the SW response is positive over the colder ocean areas, as the colder ocean favors less shading by convective clouds. This indicates that the SST response is partly damped by changes in overshooting deep convection. LH flux also responds to the SST changes, and mostly works to damp the SST response. Compared to SW and LH fluxes, the effect of the LW and SH (not shown) on the net surface heat flux changes is small.

3.1.2. *CPE* ensemble

In the initial stage associated with the fast land cooling during two or three months after the eruption, Figure 6j shows, in contrast to the *NTE* ensemble, a weak negative surface temperature response in the EP for the *CPE* ensemble. This is because the LOTG mechanism develops not only in the WP but also in the EP, since the control EP SST and nearby land are warmer than normal (see Figure 2b) despite the maximum SST is in the CP, thus enhancing westerly (easterly) wind anomaly in the WP (EP) (Figure 6k). This causes an eastward transport of warm water in the WP and intensification of the upwelling and cooling SST in the EP. As in the *NTE* ensemble, this effect is short-lived. In the WP the net-flux cooling of ocean in 1991 (Figure 6l) turns on the ODT mechanism [Seager *et al.*, 1988; Clement *et al.*, 1996] starting from October 1991. Due to the CP position of the warm pool in the *CPE* case, the upwelling is partially suppressed, but still functions. Therefore, the ODT mechanism is slightly weaker in the *CPE* case than in the *NTE* case, but still is relatively long-lasting. The positive SST response survives until the end of 1992, slightly shorter than in *NTE* case. As in the *NTE* ensemble, an eastward shift of deep convection (Figure 6o) enhances the response.

The westerly wind response, driven by the weakened WP SST gradient, pushes the equatorial Pacific towards El Niño-like conditions (as in the *NTE* case) and warms the EP SST (Figure 6j,k). The volcanically induced warming in the EP finally shuts down the upwelling and ODT in February of 1993. As in the *NTE* case, the cloudiness and net surface energy fluxes tend to damp the SST response (PRT-CTR) after May 1992.

According to the observational study by *Li et al.* [2010], at the time of the Mt Pinatubo eruption the moderate CP El Niño of 1991 also transitioned to EP in 1992, similar to what we find in our *CPE* simulations.

3.1.3. *EPE* ensemble

The SST and atmospheric responses of the *EPE* case significantly deviate from those of the *CPE* and *NTE* cases. A much more pronounced EP cooling that starts soon after the eruption and lasts for more than half a year is a distinct feature of the *EPE* response (Figure 6r). A newly-developed zonal SST gradient enhances the trade winds in the CP (Figure 6s), boosting the upwelling and facilitating a prompt westward expansion of the negative SST response toward the CP in October 1991 – February 1992. At the same time, similar to the *NTE* and *CPE* cases, the westerly wind response develops in the WP initially due to the LOTG mechanism and later due to the ODT mechanism. This gradually leads to a relaxation of the negative temperature response in the CP and EP, causing a positive SST response in May-September 1992. Because of the weak ODT and deficit of available heat content in the *EPE* case, due to the shutdown of background upwelling and the poleward discharge of heat content associated with the strong El Niño, the westerly wind anomaly is short-lived and vanishes by the end of summer 1992 (Figure 6s). Thus, the El Niño-like signal is shorter than that in the *NTE* and *CPE* cases.

The cloud cover in the *EPE* case is the broadest among all the cases, but it responds relatively moderately, except for a strong decline in EP and CP in 1991 (Figure 6w). Due to the EP SST cooling in the second half of 1991, both the deep convection zone and cloudiness anomaly decline in the EP (Figure 6w). In the first half of 1992 the colder EP SST leads to the westward shift of convection and precipitation, reducing the amount of clouds in the EP, and increasing downward SW radiation (Figure 6u). Generally in all cases, the SW flux mainly responds to cloud changes, which increase where SST warms and decrease where it cools, effectively damping the SST response (Figure 6e,m,u).

Finally, we consider the ocean heat content response, which is less affected by the direct surface cooling caused by volcanic radiative forcing. Figure 6h,p,x show the response (PRT-CTR) of the top 300 m ocean heat content of the 2°S-2°N averaged equatorial Pacific region. It demonstrates roughly the same effects, discussed above in Sections 3.1.1 and 3.1.2 using SST changes as diagnostics, but more clearly defines the termination of different development phases. Positive responses of the ocean heat content extend to the end of 1992 for the *NTE* case, and the end of 1993 for the *CPE* case. In both cases, the ODT effects are evident until the end of the warming phase. For the *EPE* case, in contrast, we see a significant negative ocean heat content response in the EP that lasts until the end of 1991.

Because the strong background El Niño warms SSTs in the EP already at the time of eruption and later on (see Figure 2c), the sea and land surface temperatures near the South American continent are much higher in the *EPE* than in *CPE* and *NTE* cases. When the land surface temperature in the EP decreases after the eruption, the EP LOTG is stronger than in *NTE* or *CPE* cases due to the anomalously warm coastal waters.

However, because of the land's low thermal capacity, the LOTG effect is short-lived as in *NTE* and *CPE* cases, and cannot maintain the negative temperature response beyond half a year after the eruption (Figure 6r). This is further clarified in Sections 3.3 and 3.4.

3.2. Ocean Heat Budget

To better understand the interplay of different processes and compare their contributions in changing the mixed layer temperature and heat content, we analyze the ocean mixed layer heat budget using the equation for mixed layer temperature from *Stevenson and Niiler* [1983] and *Huang et al.* [2010] to calculate monthly mean ocean temperature tendencies:

$$\frac{dT_a}{dt} = -w_H \frac{T_a - T_H}{H} - u_a \frac{\partial T_a}{\partial x} - v_a \frac{\partial T_a}{\partial y} + \frac{Q_{NF}}{\rho C_p H} + Q_{Res} \quad (1)$$

where T_a , u_a and v_a are the temperature, zonal and meridional currents; subscript a denotes the quantities vertically averaged between surface and the bottom of the mixed layer at $H=50$ m; T_H and w_H are the temperature and ocean vertical velocity at $H=50$ m, Q_{NF} is net surface heat flux, $\rho=1029$ kg m⁻³ is the seawater density, and $C_p=3990$ J kg⁻¹ K⁻¹ is the specific heat capacity of seawater at constant pressure. The first term in the right side of Equation (1) denotes the thermocline and ODT effect, the second and third terms are zonal and meridional advection, the fourth term is heating/cooling caused by surface heat fluxes, Q_{Res} is a residual term which includes vertical diffusion and subgridscale mixing.

Each element of the heat budget is integrated over the narrowed Niño3 + Niño4 region (2°S-2°N 160°E-90°W) for the perturbed and control ensembles, and the difference

response is presented in Figure 7. The results are shown for five half-year periods: a) July-December 1991; b) January-June 1992; c) July-December 1993; d) January-June 1993, and e) July-December 1993.

During period *a* (Figure 7a), the mixed layer responds to the radiative cooling and the change of the surface wind stresses induced by the increased LOTG and slowly developing ODT and Bjerknes feedbacks. The upper ocean warms only for *NTE*, while the strongest cooling happens in *EPE* due to zonal and meridional advective cooling in the EP.

Figure 7b shows the important stage of strengthening of the El Niño-like response due to the volcanic impact. Period *b* in the control *CPE* and *EPE* ensembles corresponds to the transition from El Niño to La Niña. However, due to the strong ocean dynamical response to volcanic forcing, an intense warming is observed in all cases even though the surface fluxes tend to damp the temperature anomalies. In the *NTE* and *CPE* cases, all three advective terms contribute roughly equally to this warming. In contrast, the *EPE* warming is mostly caused by the thermocline effect. Zonal and meridional advection also contribute to this warming, but to a lesser extent.

During period *c*, in all cases the El Niño-like responses enter a decay phase, which is the fastest in the *EPE* ensemble due to a fast transition from a strong El Niño into a strong La Niña, mostly caused by upwelling of anomalously cold water due to arrival of an upwelling oceanic Kelvin wave.

During period *d*, the *CPE* cooling is caused by a strong zonal advection feedback. The *NTE* case reaches the final relaxation state at a later time than *CPE* (period *e*) by means of the almost equal contributions of the thermocline and zonal advection feedbacks.

3.3. Initial ENSO responses in period a

The initial stage of the ENSO response (period a in Figure 7) is characterized by competition between the LOTG and ODT mechanisms, and reveals drastic differences between the *EPE* and *NTE/CPE* SST responses. To better demonstrate the onsets of the LOTG and ODT mechanisms and differences in the SST evolution in *NTE*, *CPE* and *EPE* cases, in Figure 8 we show maps of the monthly 10-member ensemble mean responses (PRT-CTR) of surface temperature and wind stress for all experiments for July-December of 1991. The left column of Figure 8 corresponds to the *NTE* experiment, the middle to the *CPE*, and the right to the *EPE*. In all cases, the land mass cooling is present in Australia and the Americas, although it is partially opposed by advection of warm air from the ocean as happens in the *NTE* in July and November, in *CPE* in July, and in *EPE* in August, November, and slightly in October 1991.

In the *NTE* and *CPE* ensembles, both WP and EP LOTG effects on equatorial (5°S - 5°N) wind stress are seen in August-September. The WP SST cooling onset associated with the ODT mechanism takes place in October and November 1991 in the *CPE* and *NTE* experiments, respectively, and develops a westerly wind stress response in the WP and CP (Figure 8d,e,j,k).

In the *EPE* experiment, we see the strong off-land wind stress response in July 1991 (Figure 8m). The significant SST cooling of the EP starts from August 1991 (Figure 8n). This SST cooling is so strong that it initiates a significant positive feedback of the wind stress in the CP in September-December, and continues to expand westward (Figure 8o-r). At the same time, the ODT mechanism turns on in October 1991 (Figure 8p). As we mentioned earlier, the strong EP cooling in the *EPE* case cannot be fully explained

by only LOTG and ODT mechanisms. Our working hypothesis is that this ocean cooling is partially caused by the predominant weakening of the strong El Niños in the perturbed *EPE* ensemble. This effect was discussed by *Wittenberg et al.* [2014] and based on the asymmetry of a strong El Niño response probability distribution function. It essentially means that a very strong El Niño disturbed by any perturbation more probably leads to an outcome of a weaker El Niño. To better quantify this effect, a specific set of sensitivity experiments are conducted and analyzed in the Section 3.4.

3.4. Sensitivity of El Niño response to small perturbations

Wittenberg et al. [2014] demonstrated that El Niño is very sensitive to the small perturbations that limit its predictability. In their simulations, a slight perturbation of ICs at the beginning of a calendar year drastically affected the El Niño later in the year and onwards. Stricken by the IC change, the sporadically developing WWBs stochastically impacted the amplitude of El Niño and were even able to reverse the ENSO phase with respect to the unperturbed case. At first glance, this contradicts our observation of a statistically significant ENSO response to volcanic forcing in the *EPE* and *CPE* ensembles, and has to be explained. In addition, this stochastic behaviour could be useful to understand the initial stage of the *EPE* ensemble development, as the stochastic component of the response might be responsible for the initial drastic cooling in the *EPE* case, as we hypothesized in Section 3.3.

Therefore, in this section we specifically test the sensitivity of the El Niño response to small perturbations in the control and perturbed runs. We use a single IC, which results in a strong EP El Niño in the initial year of the simulation (Figure 9, black dashed line). We name this control simulation CTR_0 . The perturbations are introduced by a small radiative

forcing that is generated by imposing the Pinatubo aerosol extinctions [*Sato et al.*, 1993; *Stenchikov et al.*, 2009] multiplied by a factor α , where α ranges from 0.001 to 0.05 with a step of 0.001. The corresponding SW radiative forcings scale proportionally. We apply these small perturbations in the control runs with zero background volcanic forcing and in the perturbed runs on the top of the full-scale Pinatubo forcing. In both perturbed and control runs, the small forcing is imposed at the beginning of 1991 (in our case in February), as in *Wittenberg et al.* [2014], and in June, at the time of the actual observed Pinatubo eruption. We assume that forcing imposed early in the year has more time to disrupt the control El Niño, than that imposed in June.

In order to evaluate the spread of responses to these small perturbations, we calculate two sets of 50-member “perturbed control” and “perturbed Pinatubo” ensembles, named CTR_{α}^{Feb} , CTR_{α}^{Jun} , PRT_{α}^{Feb} , PRT_{α}^{Jun} , respectively (see Table 2). Thus, in “June” cases we preserve the control El Niño until the time of a perturbation, so the control El Niño develops unaffected until a perturbation is imposed. In “February” cases, the El Niño is actually first affected in January, due to time interpolation of the prescribed volcanic optical depth.

Figure 9 compares the changes of Niño 3.4 index in all four ensembles forced by α perturbations imposed in February (upper panel) and in June (lower panel) at the time of Pinatubo eruption. Perturbations imposed in February lead to a drastic change of the Niño 3.4 index, almost completely suppressing the strong EP El Niño in most members of the CTR_{α}^{Feb} and PRT_{α}^{Feb} ensembles, while the June perturbations in CTR_{α}^{Jun} runs disturb the El Niño only slightly. The ensemble average in PRT_{α}^{Jun} runs repeats the main

features of the Niño 3.4 response revealed in Figure 5c, confirming the statistical stability of our 10-member ensemble ENSO responses.

Thus, the small α perturbations imposed in June do not have enough time to grow and affect the ENSO phase in the current and next year (Figure 9b). Although the variability inside the CTR_{α}^{Jun} ensemble grows in the second year after perturbation, the ensemble mean still captures the El Niño trajectory fairly well. However, the February perturbations change ENSO drastically. Experiments conducted imposing disturbances in different months (not shown) suggest that the signal-to-noise ratio in case of winter and spring eruptions is smaller than in the case of summer and fall eruptions, i.e. the ENSO response to eruptions like El Chichón or Tambora in April (apart from the response dependence on the magnitude of an eruption) could be less pronounced than that of Pinatubo which happened later in the year. This finding is consistent with the concept of the “ENSO spring predictability barrier”, which suggests that the persistence of El Niño is lower during the late boreal winter and spring, while it increases starting in June. McPhaden [2003] examined this concept in the observations and Levine and McPhaden [2015] confirmed it using a simplified conceptual model, while our study finds consistent behavior in a coupled ocean-atmosphere GCM.

Another interesting feature in Figure 9 is a decrease of the Niño 3.4 index in both CTR_{α}^{Jun} and PRT_{α}^{Jun} ensembles with respect to the CTR_0 at the peak of El Niño in November-December 1991. This effect is directly related to the drastic SST cooling in the *EPE* case shown in Figure 8 and discussed in Section 3.3. It is also consistent with the results from our 10-member ensemble (Figure 5c). To clarify this issue, in Figure 10 we present the 50-member ensemble mean monthly surface temperature responses calcu-

lated from PRT_{α}^{Jun} and CTR_{α}^{Jun} experiments with respect to CTR_0 , and their difference ($PRT_{\alpha}^{Jun} - CTR_{\alpha}^{Jun}$). The idea is to split up the “perturbed Pinatubo” (left column) response into the stochastic (middle column) and the forced deterministic volcanic (right column) components.

Black dots in Figure 10a-f,g-l (left and middle columns) show the areas where the CTR_0 surface temperature is below the 10th percentile or above the 90th percentile of the PRT_{α}^{Jun} (left column) and CTR_{α}^{Jun} (central column) ensembles, respectively. We choose to use percentiles here because the probability distributions of both PRT_{α}^{Jun} and CTR_{α}^{Jun} ensembles are skewed as discussed above. In Figure 10m-r (right column) black dots show statistically significant $PRT_{\alpha}^{Jun}-CTR_{\alpha}^{Jun}$ surface temperature responses at the 0.05 significance level, calculated using a two-tailed Student’s t-test, as their probability distribution is close to normal.

The magnitude of the stochastic response in the EP is evident in Figure 10g-l (central column), which shows the purely chaotic dispersion of the unforced ensemble. The anomaly is predominantly negative in the equatorial region, indicating a shift to weaker El Niños.

The volcanically induced SST cooling with the stochastic component removed (Figure 10m-r) is statistically significant, and reaches more than 1 K in the equatorial region. The “deterministic” SST cooling (Figure 10m-r) is slightly greater than the stochastic cooling caused by the infinitesimal forcing (Figure 10m-r).

In order to better separate the radiative and dynamical feedbacks in July-December 1991 for this single EPE case, we performed the ocean heat budget analysis using differences of PRT_{α}^{Jun} and CTR_{α}^{Jun} ensembles (i.e., removing the stochastic component of the

response) as described in Section 3.2, but for two 3-month intervals. Figure 11 shows that during the first three months (July-September, 1991) of the radiative cooling, the zonal and meridional advection along with the thermocline feedbacks strengthen the cooling in the EP. Starting from October 1991 the ODT overwhelms this, and, despite the intensified radiative cooling, the mixed layer warms due to thermocline and zonal advection feedbacks.

4. Discussion and Conclusions

This research article focuses on mechanisms of the response of ENSO to Pinatubo-size volcanic forcing, and aims to reconcile apparent inconsistencies in previous studies [*Mann et al.*, 2005; *Emile-Geay et al.*, 2008; *McGregor and Timmermann*, 2011; *Ohba et al.*, 2013].

Using the coupled ocean-atmosphere model CM2.1, we simulate the climate impact of a Pinatubo-size eruption in ENSO-neutral, CP and EP El Niño, and La Niña years. We show that the initial ENSO phase, El Niño amplitude and type, and the seasonal timing of the eruption affect the climate and ENSO responses to volcanic forcing. We find that the eruption causes different climate responses in CP and EP El Niño years, and we study the sensitivity of the volcano-induced ENSO response to small perturbations, illuminating the contributions of stochastic and deterministic responses to volcanic radiative forcing.

4.1. ENSO Response

A Pinatubo-size eruption induces an El Niño-like response in the first year after the eruption in ENSO-neutral years, and prolongs moderate CP El Niños. The EP El Niño weakens due to a combined effect of the enhanced LOTG mechanism and the ENSO stochastic response, and its termination is delayed. The ENSO in La Niña years is largely

insensitive to volcanic forcing in CM2.1. The absence of any La Niña response is caused by a weak LOTG mechanism due to the anomalously cold equatorial SST, and suppressed ODT mechanism because of the weak zonal upwelling gradient in the entire equatorial Pacific. This effect might be exaggerated by CM2.1, as its La Niñas tend to expand upwelling farther west than observed.

4.2. Deterministic Mechanisms

The LOTG mechanism described by *Ohba et al.* [2013] as the main driver of the ENSO response to volcanic forcing is also at work in CM2.1. However, we find it to be relatively short-lived and work only for the first 2-3 months after the eruption, being the forerunner of stronger dynamical responses. Depending on the ENSO phase, the LOTG enhances wind anomalies in the WP and/or EP. During the response of neutral ENSO or CP El Niño, the WP westerly wind anomaly dominates and causes an El Niño-like warming in the perturbed experiments. In the response of the EP El Niño the EP easterly wind anomaly prevails, although it is not fully related to the LOTG mechanism. Taking into account the findings of *Wittenberg et al.* [2014] and using the “perturbed forcing” technique, we find that the total cooling response during the first six months after an eruption is a combination of stochastic and deterministic components.

The ODT mechanism of *Clement et al.* [1996] takes over after the LOTG in October-November 1991, maintaining a deterministic El Niño-like response for a year in the CP El Niño case, and almost two years in the ENSO-neutral case. In the *EPE* case, weakened upwelling due to the strong El Niño tempers the ODT, resulting in only short-term SST warming.

4.3. Stochastic Mechanisms

Wittenberg et al. [2014] indicated the high sensitivity of El Niños to small perturbations that limits their predictability. In particular, our sensitivity analysis suggests that the eruption response of the strong EP El Niño contains both stochastic and deterministic components. The role of the stochastic component is large if small perturbations are imposed at the beginning of the calendar year, but decreases if disturbances are imposed later in the year. Because the Pinatubo eruption occurred in June, the deterministic part of the EP El Niño response prevails over the stochastic one. This suggests that the timing of a volcanic eruption is critical for the El Niño response. The EP El Niño responses to volcanic eruptions occurring in the winter-spring are more contaminated by chaotic dispersion than those occurring in summer-fall. Therefore, Pinatubo-size eruptions in winter and spring are less likely to produce a clean impact on strong EP El Niños than the actual Pinatubo, which occurred in June. In this context, the conclusion in *Robock et al.* [1995] that the huge “El Niño of the century” in 1982 after the El Chichón eruption in April could not be significantly influenced by volcanic forcing, as it was already in the development phase at the time of eruption, might be questioned.

4.4. Consistency With Other Studies and Observations

Our results are consistent with the findings by *Ohba et al.* [2013] in terms of development of an El Niño-like response in the first year after a Pinatubo-size eruption. However, they did not consider different flavors of El Niño. In addition, the La Niña in the CM2.1 does not show a tendency toward warmer ocean conditions after the eruption, unlike in the MIROC5i model used by *Ohba et al.* [2013].

The responses of different El Niño types - CP and EP in our study - are consistent, even quantitatively, with the ERSST observational data displayed in Figure 1 and discussed in *Li et al.* [2010] and *Wahl et al.* [2014]. The strong EP El Niño at the time of the El Chichón eruption was comparatively short and followed by a La Niña, while the moderate CP El Niño during the Pinatubo eruption lasted longer and transformed from CP to EP in the second year after the eruption, as seen in our simulations. In fact, a La Niña-like response often follows the El Niño-like response [*Maher et al.*, 2015], which we have not fully addressed in this study, which has focused on the immediate post-eruption period. The induced La Niña-like response will be a subject of a different study.

As Pinatubo-size volcanic impacts in ENSO-neutral and CP El Niño years generate El Niño like responses in at least the first year after an eruption, the frequency of El Niño conditions in this year might reach 0.65 (see Table 1: $NTE + CPE$). This is consistent with paleo analyses that suggest a doubling of the probability of warm EP SSTs in post-eruption years, compared to the model climatology (0.27, see Table 1: $CPE + EPE$).

4.5. Recommendations for Further Analysis

We have demonstrated a sensitivity of the volcanic response to the magnitude and shape of an ENSO event that otherwise would have developed in the unperturbed case. This might partially explain the spread of previous model results, as simulations in different studies have been conducted for different initial ENSO phases. Moreover, many up-to-date models produce only one type of El Niño, or produce unrealistically weak or overly frequent ENSO events [*Ham and Kug*, 2012; *Yu and Kim*, 2010]. This intrinsic model behavior inevitably affects the simulated ENSO sensitivity, and may not be able to completely cover the full set of possible cases in nature.

We suggest that when analyzing the ENSO sensitivity to volcanic eruptions in models or observations, special attention needs to be paid to the initial phase of ENSO and the seasonal timing of the eruption. Previous studies did not take into account that composites of different initial ENSO phases, eruption timings. *Meehl et al.* [2015] also noted that especially multimodel composites could obscure the ENSO response signals. Moreover, as in a specific model one perturbs an intrinsic ENSO, the results inevitably become model dependent, as different models generate different (and often inadequate) ENSO cycles [*Gabriel and Robock*, 2015], so meaningful composites are difficult to obtain.

The numerical experiments we conducted are consistent with those proposed in the “volc-pinatubo-full” task from the VolMIP activity planned for CMIP6 [*Zanchettin et al.*, 2016] and will be contributing to that intercomparison study. Our recommendations for a more accurate and selective compositing of the results will help to better identify the ENSO responses to volcanic forcing. The “volc-pinatubo-slab” experimental design [*Zanchettin et al.*, 2016], however, is insufficient to cover all aspects of Volcano-ENSO interaction, as a full ocean model is needed.

Acknowledgments. We thank Hans-F. Graf, Alan Robock and Jim Carton for valuable discussions. The research reported in this publication was supported by King Abdullah University of Science and Technology. In particular, for computer time, the resources of the KAUST Supercomputing Laboratory were used, in addition to those of NOAA GFDL. The simulation results and supporting datasets are available from the corresponding author upon request. NOAA ERSST V4 data are provided by the NOAA/OAR/ESRL PSD, Boulder, Colorado, USA, from their Web site at <http://www.esrl.noaa.gov/psd/>

References

- Adams, J. B., M. E. Mann, and C. M. Ammann (2003), Proxy evidence for an El Niño-like response to volcanic forcing, *Nature*, *426*(6964), 274–278.
- Anderson, J. L., V. Balaji, A. J. Broccoli, W. F. Cooke, et al. (2004), The new GFDL global atmosphere and land model AM2-LM2: Evaluation with prescribed sst simulations, *Journal of Climate*, *17*(24), 4641.
- Ashok, K., S. K. Behera, S. A. Rao, H. Weng, and T. Yamagata (2007), El Niño Modoki and its possible teleconnection, *Journal of Geophysical Research: Oceans* (1978–2012), *112*(C11).
- Atwood, A. R., D. S. Battisti, A. T. Wittenberg, W. G. H. Roberts, and D. J. Vimont (2016), Characterizing unforced multi-decadal variability of ENSO: A case study with the GFDL CM2.1 coupled GCM, *Climate Dyn.*, submitted.
- Bjerknes, J. (1969), Atmospheric teleconnections from the Equatorial Pacific, *Monthly Weather Review*, *97*(3), 163–172.
- Briffa, K. R., P. D. Jones, F. H. Schweingruber, and T. J. Osborn (1998), Influence of volcanic eruptions on Northern Hemisphere summer temperature over the past 600 years, *Nature*, *393*(6684), 450–455.
- Brönnimann, S., E. Xoplaki, C. Casty, A. Pauling, and J. Luterbacher (2007), ENSO influence on europe during the last centuries, *Climate Dynamics*, *28*(2-3), 181–197.
- Capotondi, A., A. T. Wittenberg, M. Newman, E. Di Lorenzo, J.-Y. Yu, P. Braconnot, J. Cole, B. Dewitte, B. Giese, E. Guilyardi, et al. (2015), Understanding ENSO diversity, *Bulletin of the American Meteorological Society*, *96*, 921–938, doi:10.1175/BAMS-D-13-00117.1.

Cash, D. W., J. C. Borck, and A. G. Patt (2006), Countering the loading-dock approach to linking science and decision making comparative analysis of El Niño/Southern Oscillation (ENSO) forecasting systems, *Science, Technology & Human Values*, 31(4), 465–494.

Chavez, F. P., J. Ryan, S. E. Lluch-Cota, and M. Niquen (2003), From anchovies to sardines and back: multidecadal change in the Pacific Ocean, *Science*, 299(5604), 217–221.

Chen, C., M. A. Cane, A. T. Wittenberg, and D. Chen (2016), ENSO in the CMIP5 simulations: Lifecycles, diversity, and responses to climate change, *Journal of Climate*, submitted.

Chen, D., T. Lian, C. Fu, M. A. Cane, Y. Tang, R. Murtugudde, X. Song, Q. Wu, and L. Zhou (2015), Strong influence of westerly wind bursts on El Niño diversity, *Nature Geoscience*, 8(5), 339–345.

Choi, K.-Y., G. A. Vecchi, and A. T. Wittenberg (2013), ENSO transition, duration, and amplitude asymmetries: Role of the nonlinear wind stress coupling in a conceptual model, *Journal of Climate*, 26(23), 9462–9476.

Choi, K.-Y., G. A. Vecchi, and A. T. Wittenberg (2015), Nonlinear zonal wind response to ENSO in the CMIP5 models: Roles of the zonal and meridional shift of the ITCZ/SPCZ and the simulated climatological precipitation, *Journal of Climate*, 28(21), 8556–8573.

Church, J. A., N. J. White, and J. M. Arblaster (2005), Significant decadal-scale impact of volcanic eruptions on sea level and ocean heat content, *Nature*, 438(7064), 74–77.

Clement, A. C., R. Seager, M. A. Cane, and S. E. Zebiak (1996), An ocean dynamical thermostat, *Journal of Climate*, 9(9), 2190–2196.

Collins, M., S.-I. An, W. Cai, A. Ganachaud, E. Guilyardi, F.-F. Jin, M. Jochum, M. Lengaigne, S. Power, A. Timmermann, G. Vecchi, and A. Wittenberg (2010), The impact of global warming on the tropical Pacific Ocean and El Niño, *Nature Geoscience*, 3(6), 391–397.

D’Arrigo, R., E. R. Cook, R. J. Wilson, R. Allan, and M. E. Mann (2005), On the variability of ENSO over the past six centuries, *Geophysical Research Letters*, 32(3), n/a–n/a, doi:10.1029/2004GL022055.

De Silva, S. L., and G. A. Zielinski (1998), Global influence of the ad 1600 eruption of Huaynaputina, Peru, *Nature*, 393(6684), 455–458.

Delworth, T. L., A. J. Broccoli, A. Rosati, R. J. Stouffer, V. Balaji, J. A. Beesley, W. F.

Cooke, K. W. Dixon, J. Dunne, K. Dunne, et al. (2006), GFDL’s CM2 global coupled climate models. Part I: Formulation and simulation characteristics, *Journal of Climate*, 19(5), 643–674.

DiNezio, P. N., B. P. Kirtman, A. C. Clement, S.-K. Lee, G. A. Vecchi, and A. Wittenberg (2012), Mean climate controls on the simulated response of ENSO to increasing greenhouse gases, *Journal of Climate*, 25, 7399–7420, doi:10.1175/JCLI-D-11-00494.1.

Dutton, E. G., and J. R. Christy (1992), Solar radiative forcing at selected locations and evidence for global lower tropospheric cooling following the eruptions of El Chichón and Pinatubo, *Geophysical Research Letters*, 19(23), 2313–2316.

Emile-Geay, J., R. Seager, M. A. Cane, E. R. Cook, and G. H. Haug (2008), Volcanoes and ENSO over the past millennium, *Journal of Climate*, 21(13), 3134–3148.

Emile-Geay, J., K. Cobb, M. Mann, and A. T. Wittenberg (2013), Estimating central equatorial Pacific SST variability over the past millennium. Part II: Reconstructions

and implications, *Journal of Climate*, 26, 2329–2352, doi:10.1175/JCLI-D-11-00511.1.

Fang, X.-H., F. Zheng, and J. Zhu (2015), The cloud radiative effect when simulating strength asymmetry in two types of El Niño events using CMIP5 models, *Journal of Geophysical Research: Oceans*.

Fischer, E., J. Luterbacher, E. Zorita, S. Tett, C. Casty, and H. Wanner (2007), European climate response to tropical volcanic eruptions over the last half millennium, *Geophysical Research Letters*, 34(5).

Gabriel, C., and A. Robock (2015), Stratospheric geoengineering impacts on El Niño/Southern Oscillation, *Atmospheric Chemistry and Physics*, 15(20), 11,949–11,966.

Gebbie, G., I. Eisenman, A. Wittenberg, and E. Tziperman (2007), Modulation of westerly wind bursts by sea surface temperature: A semistochastic feedback for ENSO, *Journal of Atmospheric Science*, 64, 3281–3295, doi:10.1175/JAS4029.1.

Gleckler, P., T. Wigley, B. Santer, J. Gregory, K. AchutaRao, and K. Taylor (2006), Volcanoes and climate: Krakatoa's signature persists in the ocean, *Nature*, 439(7077), 675–675.

Gnanadesikan, A., K. W. Dixon, S. M. Griffies, V. Balaji, M. Barreiro, J. A. Beesley, W. F. Cooke, T. L. Delworth, R. Gerdes, M. J. Harrison, et al. (2006), GFDL's CM2 global coupled climate models. Part II: the baseline ocean simulation, *Journal of Climate*, 19(5), 675–697.

Goldenberg, S. B., C. W. Landsea, A. M. Mestas-Núñez, and W. M. Gray (2001), The recent increase in atlantic hurricane activity: Causes and implications, *Science*, 293(5529), 474–479.

Graf, H.-F., and D. Zanchettin (2012), Central Pacific El Niño, the “subtropical bridge,” and Eurasian climate, *Journal of Geophysical Research: Atmospheres* (1984–2012), *117*(D1).

Gray, W. M. (1984), Atlantic seasonal hurricane frequency. Part I: El Niño and 30 mb quasi-biennial oscillation influences, *Monthly Weather Review*, *112*(9), 1649–1668.

Griffies, S., A. Gnanadesikan, K. W. Dixon, J. Dunne, R. Gerdes, M. J. Harrison, A. Rosati, J. Russell, B. L. Samuels, M. J. Spelman, et al. (2005), Formulation of an ocean model for global climate simulations, *Ocean Science*, *1*(1), 45–79.

Guilyardi, E., A. Wittenberg, M. Balmaseda, W. Cai, M. Collins, M. J. McPhaden, M. Watanabe, and S.-W. Yeh (2016), Fourth CLIVAR workshop on the evaluation of ENSO processes in climate models: ENSO in a changing climate, *Bulletin of the American Meteorological Society*, *97*(5), 817–820, doi:10.1175/BAMS-D-15-00287.1.

Ham, Y.-G., and J.-S. Kug (2012), How well do current climate models simulate two types of El Niño?, *Climate dynamics*, *39*(1-2), 383–398.

Hansen, J., A. Lacis, R. Ruedy, and M. Sato (1992), Potential climate impact of Mount Pinatubo eruption, *Geophysical Research Letters*, *19*(2), 215–218, doi:10.1029/91GL02788.

Hansen, J., M. Sato, R. Ruedy, et al. (1997), Radiative forcing and climate response, *Journal of Geophysical Research*, *102*, 6831–6864.

Haywood, J. M., A. Jones, N. Bellouin, and D. Stephenson (2013), Asymmetric forcing from stratospheric aerosols impacts Sahelian rainfall, *Nature Climate Change*, *3*(7), 660–665.

Hirono, M. (1988), On the trigger of El Niño Southern Oscillation by the forcing of early El Chichon volcanic aerosols, *Journal of Geophysical Research: Atmospheres (1984–2012)*, *93*(D5), 5365–5384.

Huang, B., Y. Xue, D. Zhang, A. Kumar, and M. J. McPhaden (2010), The NCEP GODAS ocean analysis of the tropical Pacific mixed layer heat budget on seasonal to interannual time scales, *Journal of Climate*, *23*(18), 4901–4925.

Huang, B., V. F. Banzon, E. Freeman, J. Lawrimore, W. Liu, T. C. Peterson, T. M. Smith, P. W. Thorne, S. D. Woodruff, and H.-M. Zhang (2015), Extended reconstructed sea surface temperature version 4 (ersst. v4). part i: upgrades and intercomparisons, *Journal of Climate*, *28*(3), 911–930.

Ineson, S., and A. Scaife (2009), The role of the stratosphere in the European climate response to El Niño, *Nature Geoscience*, *2*(1), 32–36.

Jia, L., X. Yang, G. A. Vecchi, R. G. Gudgel, T. L. Delworth, A. Rosati, W. F. Stern, A. T. Wittenberg, L. Krishnamurthy, S. Zhang, et al. (2015), Improved seasonal prediction of temperature and precipitation over land in a high-resolution GFDL climate model, *Journal of Climate*, *28*(5), 2044–2062.

Karamperidou, C., M. A. Cane, U. Lall, and A. T. Wittenberg (2014), Intrinsic modulation of ENSO predictability viewed through a local Lyapunov lens, *Climate Dynamics*, *42*, 253–270, doi:10.1007/s00382-013-1759-z.

Kessler, W. S., and M. J. McPhaden (1995), The 1991–1993 El Niño in the central Pacific, *Deep Sea Research Part II: Topical Studies in Oceanography*, *42*(2), 295–333.

Kim, S. T., and F.-F. Jin (2011), An ENSO stability analysis. Part II: results from the twentieth and twenty-first century simulations of the CMIP3 models, *Climate Dynamics*,

36(7-8), 1609–1627.

Kim, S. T., W. Cai, F.-F. Jin, A. Santoso, L. Wu, E. Guilyardi, and S.-I. An (2014), Response of El Niño sea surface temperature variability to greenhouse warming, *Nature Climate Change*, 4(9), 786–790.

Kug, J.-S., J. Choi, S.-I. An, F.-F. Jin, and A. T. Wittenberg (2010), Warm pool and cold tongue El Niño events as simulated by the GFDL 2.1 coupled GCM, *Journal of Climate*, 23(5), 1226–1239.

Lacis, A., J. Hansen, and M. Sato (1992), Climate forcing by stratospheric aerosols, *Geophysical Research Letters*, 19(15), 1607–1610.

Lamb, H. H. (1970), Volcanic dust in the atmosphere; with a chronology and assessment of its meteorological significance, *Philosophical Transactions of the Royal Society of London A: Mathematical, Physical and Engineering Sciences*, 266(1178), 425–533.

Lee, S.-K., P. N. DiNezio, E.-S. Chung, S.-W. Yeh, A. T. Wittenberg, and C. Wang (2014), Spring persistence, transition, and resurgence of El Niño, *Geophysical Research Letters*, 41(23), 8578–8585, doi:10.1002/2014GL062484.

Lee, S.-K., A. T. Wittenberg, D. B. Enfield, S. J. Weaver, C. Wang, and R. Atlas (2016), US regional tornado outbreaks and their links to spring ENSO phases and North Atlantic SST variability, *Environmental Research Letters*, 11(4), 044,008.

LeGrande, A. N., K. Tsigaridis, and S. E. Bauer (2016), Role of atmospheric chemistry in the climate impacts of stratospheric volcanic injections, *Nature Geoscience*.

Levine, A. F. Z., and M. J. McPhaden (2015), The annual cycle in enso growth rate as a cause of the spring predictability barrier, *Geophysical Research Letters*, 42(12), 5034–5041, doi:10.1002/2015GL064309, 2015GL064309.

- Li, G., B. Ren, C. Yang, and J. Zheng (2010), Indices of El Niño and El Niño Modoki: An improved El Niño Modoki index, *Advances in Atmospheric Sciences*, *27*, 1210–1220.
- Li, J., S.-P. Xie, E. R. Cook, G. Huang, R. D'Arrigo, F. Liu, J. Ma, and X.-T. Zheng (2011), Interdecadal modulation of El Niño amplitude during the past millennium, *Nature Climate Change*, *1*(2), 114–118.
- Li, J., S.-P. Xie, E. R. Cook, M. S. Morales, D. A. Christie, N. C. Johnson, F. Chen, R. D'Arrigo, A. M. Fowler, X. Gou, et al. (2013), El niño modulations over the past seven centuries, *Nature Climate Change*, *3*(9), 822–826.
- Lim, H.-G., S.-W. Yeh, J.-S. Kug, Y.-G. Park, J.-H. Park, R. Park, and C.-K. Song (2015), Threshold of the volcanic forcing that leads the El Niño-like warming in the last millennium: results from the ERIK simulation, *Climate Dynamics*, pp. 1–12.
- Lin, S.-J. (2004), A 'vertically Lagrangian' finite-volume dynamical core for global models, *Monthly Weather Review*, *132*(10), 2293–2307.
- Maher, N., S. McGregor, M. H. England, and A. S. Gupta (2015), Effects of volcanism on tropical variability, *Geophysical Research Letters*, *42*(14), 6024–6033.
- Mann, M. E., M. A. Cane, S. E. Zebiak, and A. Clement (2005), Volcanic and solar forcing of the tropical Pacific over the past 1000 years, *Journal of Climate*, *18*(3), 447–456.
- McCormick, M. P., L. W. Thomason, C. R. Trepte, et al. (1995), Atmospheric effects of the Mt Pinatubo eruption, *Nature*, *373*(6513), 399–404.
- McGregor, S., and A. Timmermann (2011), The effect of explosive tropical volcanism on ENSO, *Journal of Climate*, *24*(8), 2178–2191.
- McGregor, S., A. Timmermann, and O. Timm (2010), A unified proxy for ENSO and PDO variability since 1650, *Climate of the Past*, *6*(1), 1–17.

- McGregor, S., A. Timmermann, M. H. England, O. Elison Timm, and A. T. Wittenberg (2013), Inferred changes in El Niño-Southern Oscillation variance over the past six centuries, *Climate of the Past*, *9*, 2269–2284, doi:10.5194/cp-9-2269-2013.
- McPhaden, M. J. (2003), Tropical Pacific Ocean heat content variations and ENSO persistence barriers, *Geophysical Research Letters*, *30*(9).
- Meehl, G. A., H. Teng, N. Maher, and M. H. England (2015), Effects of the Mount Pinatubo eruption on decadal climate prediction skill of Pacific sea surface temperatures, *Geophysical Research Letters*, *42*(24), 10,840–10,846, doi:10.1002/2015GL066608.
- Milly, P., and A. Shmakin (2002), Global modeling of land water and energy balances. Part I: The land dynamics (LaD) model, *Journal of Hydrometeorology*, *3*(3), 283–299.
- Minnis, P., E. Harrison, L. Stowe, G. Gibson, F. Denn, D. Doelling, and W. Smith (1993), Radiative climate forcing by the Mount Pinatubo eruption, *Science*, *259*(5100), 1411–1415.
- Newhall, C. G., and S. Self (1982), The volcanic explosivity index (VEI) an estimate of explosive magnitude for historical volcanism, *Journal of Geophysical Research: Oceans* (1978–2012), *87*(C2), 1231–1238.
- Ogata, T., S.-P. Xie, A. Wittenberg, and D.-Z. Sun (2013), Interdecadal amplitude modulation of El Niño/Southern Oscillation and its impacts on tropical Pacific decadal variability, *Journal of Climate*, *26*, 7280–7297, doi:10.1175/JCLI-D-12-00415.1.
- Ohba, M., H. Shiogama, T. Yokohata, and M. Watanabe (2013), Impact of strong tropical volcanic eruptions on ENSO simulated in a coupled GCM, *Journal of Climate*, *26*(14), 5169–5182.

Otterå, O. H., M. Bentsen, H. Drange, and L. Suo (2010), External forcing as a metronome for atlantic multidecadal variability, *Nature Geoscience*, 3(10), 688–694.

Pascolini-Campbell, M., D. Zanchettin, O. Bothe, C. Timmreck, D. Matei, J. H. Jungclauss, and H.-F. Graf (2015), Toward a record of Central Pacific El Niño events since 1880, *Theoretical and Applied Climatology*, 119(1-2), 379–389.

Pausata, F. S., L. Chafik, R. Caballero, and D. S. Battisti (2015), Impacts of high-latitude volcanic eruptions on ENSO and AMOC, *Proceedings of the National Academy of Sciences*, 112(45), 13,784–13,788.

Raible, C. C., S. Brönnimann, R. Auchmann, P. Brohan, T. L. Frölicher, H.-F. Graf, P. Jones, J. Luterbacher, S. Muthers, R. Neukom, et al. (2016), Tambora 1815 as a test case for high impact volcanic eruptions: Earth system effects, *Wiley Interdisciplinary Reviews: Climate Change*.

Rasmusson, E. M., and T. H. Carpenter (1982), Variations in tropical sea surface temperature and surface wind fields associated with the southern oscillation/el niño, *Monthly Weather Review*, 110(5), 354–384.

Ratnam, J., S. Behera, Y. Masumoto, and T. Yamagata (2014), Remote effects of El Niño and Modoki events on the austral summer precipitation of southern Africa, *Journal of Climate*, 27(10), 3802–3815.

Rind, D., and A. Lacis (1993), The role of the stratosphere in climate change, *Surveys in Geophysics*, 14(2), 133–165.

Rind, D., N. Balachandran, and R. Suozzo (1992), Climate change and the middle atmosphere. Part II: The impact of volcanic aerosols, *Journal of climate*, 5(3), 189–208.

Robock, A. (2000), Volcanic eruptions and climate, *Reviews of Geophysics*, 38(2), 191–219.

Robock, A., and J. Mao (1995), The volcanic signal in surface temperature observations, *Journal of Climate*, 8(5), 1086–1103.

Robock, A., K. E. Taylor, G. L. Stenchikov, and Y. Liu (1995), GCM evaluation of a mechanism for El Niño triggering by the El Chichón ash cloud, *Geophysical Research Letters*, 22(17), 2369–2372.

Ropelewski, C. F., and M. S. Halpert (1987), Global and regional scale precipitation patterns associated with the El Niño/Southern Oscillation, *Monthly Weather Review*, 115(8), 1606–1626.

Ropelewski, C. F., and M. S. Halpert (1996), Quantifying Southern Oscillation-precipitation relationships, *Journal of Climate*, 9(5), 1043–1059.

Santer, B. D., C. Bonfils, J. F. Painter, M. D. Zelinka, C. Mears, S. Solomon, G. A. Schmidt, J. C. Fyfe, J. N. Cole, L. Nazarenko, et al. (2014), Volcanic contribution to decadal changes in tropospheric temperature, *Nature Geoscience*, 7(3), 185–189.

Sato, M., J. E. Hansen, M. P. McCormick, and J. B. Pollack (1993), Stratospheric aerosol optical depths, 1850–1990, *Journal of Geophysical Research: Atmospheres*, 98(D12), 22,987–22,994.

Schnetzler, C., G. Bluth, A. Krueger, and L. Walter (1997), A proposed volcanic sulfur dioxide index (VSI), *Journal of Geophysical Research: Solid Earth (1978–2012)*, 102(B9), 20,087–20,091.

Seager, R., S. E. Zebiak, and M. A. Cane (1988), A model of the tropical Pacific sea surface temperature climatology, *Journal of Geophysical Research: Oceans*, 93(C2), 1265–1280.

Soden, B. J. (2000), The sensitivity of the tropical hydrological cycle to ENSO, *Journal of Climate*, 13(3), 538–549.

Soden, B. J., R. T. Wetherald, G. L. Stenchikov, and A. Robock (2002), Global cooling after the eruption of Mount Pinatubo: A test of climate feedback by water vapor, *Science*, 296(5568), 727–730.

Stenchikov, G. (2009), Chapter 4 - The role of volcanic activity in climate and global change, in *Climate Change: observed impacts on planet Earth*, edited by T. M. Letcher, 1st ed., pp. 77 – 102, Elsevier.

Stenchikov, G., A. Robock, V. Ramaswamy, M. D. Schwarzkopf, K. Hamilton, and S. Ramachandran (2002), Arctic Oscillation response to the 1991 Mount Pinatubo eruption: Effects of volcanic aerosols and ozone depletion, *Journal of Geophysical Research: Atmospheres*, 107(D24).

Stenchikov, G., K. Hamilton, R. J. Stouffer, A. Robock, V. Ramaswamy, B. Santer, and H.-F. Graf (2006), Arctic Oscillation response to volcanic eruptions in the IPCC AR4 climate models, *Journal of Geophysical Research: Atmospheres (1984–2012)*, 111(D7).

Stenchikov, G., T. L. Delworth, V. Ramaswamy, R. J. Stouffer, A. Wittenberg, and F. Zeng (2009), Volcanic signals in oceans, *Journal of Geophysical Research: Atmospheres (1984–2012)*, 114(D16).

Stenchikov, G. L., I. Kirchner, A. Robock, H.-F. Graf, J. C. Antuna, R. Grainger, A. Lambert, and L. Thomason (1998), Radiative forcing from the 1991 Mount Pinatubo volcanic eruption, *Journal of Geophysical Research: Atmospheres (1984–2012)*, 103(D12), 13,837–13,857.

Stevenson, J. W., and P. P. Niiler (1983), Upper ocean heat budget during the Hawaii-to-Tahiti shuttle experiment, *Journal of physical oceanography*, *13*(10), 1894–1907.

Stevenson, S., B. Otto-Bliesner, J. Fasullo, and E. Brady (2016), “El Niño Like” hydroclimate responses to last millennium volcanic eruptions, *Journal of Climate*, *29*(8), 2907–2921.

Stevenson, S., J. Fasullo, B. Otto-Bliesner, R. Tomas, and C. Gao (2017), “The role of eruption season in reconciling model and proxy responses to tropical volcanism, *Submitted to PNAS*.

Timmreck, C. (2012), Modeling the climatic effects of large explosive volcanic eruptions, *Wiley Interdisciplinary Reviews: Climate Change*, *3*(6), 545–564.

Timmreck, C., H. Pohlmann, S. Illing, and C. Kadow (2016), The impact of stratospheric volcanic aerosol on decadal-scale climate predictions, *Geophysical Research Letters*, *43*(2), 834–842, doi:10.1002/2015GL067431.

Trenberth, K. E. (1997), The definition of El Niño, *Bulletin of the American Meteorological Society*, *78*(12), 2771–2777.

Turco, R., O. Toon, R. Whitten, P. Hamill, and R. Keesee (1983), The 1980 eruptions of Mount St. Helens: Physical and chemical processes in the stratospheric clouds, *Journal of Geophysical Research: Oceans (1978–2012)*, *88*(C9), 5299–5319.

Vecchi, G., A. Wittenberg, and A. Rosati (2006), Reassessing the role of stochastic forcing in the 1997–1998 El Niño, *Geophysical Research Letters*, *33*(1).

Vecchi, G. A., and A. T. Wittenberg (2010), El Niño and our future climate: where do we stand?, *Wiley Interdisciplinary Reviews: Climate Change*, *1*(2), 260–270.

- Vecchi, G. A., T. Delworth, R. Gudgel, S. Kapnick, A. Rosati, A. T. Wittenberg, F. Zeng, W. Anderson, V. Balaji, K. Dixon, et al. (2014), On the seasonal forecasting of regional tropical cyclone activity, *Journal of Climate*, *27*(21), 7994–8016.
- Wahl, E. R., H. F. Diaz, J. E. Smerdon, and C. M. Ammann (2014), Late winter temperature response to large tropical volcanic eruptions in temperate western North America: Relationship to ENSO phases, *Global and Planetary Change*, *122*, 238–250.
- Watanabe, M., T. Suzuki, R. O’ishi, Y. Komuro, S. Watanabe, S. Emori, T. Takemura, M. Chikira, T. Ogura, M. Sekiguchi, et al. (2010), Improved climate simulation by miroc5: mean states, variability, and climate sensitivity, *Journal of Climate*, *23*(23), 6312–6335.
- Watanabe, M., J.-S. Kug, F.-F. Jin, M. Collins, M. Ohba, and A. T. Wittenberg (2012), Uncertainty in the ENSO amplitude change from the past to the future, *Geophysical Research Letters*, *39*(20).
- Wittenberg, A. T. (2002), ENSO response to altered climates, Ph.D. thesis, Princeton University, 475pp. Available at <http://www.gfdl.noaa.gov/~atw/research/thesis>.
- Wittenberg, A. T. (2009), Are historical records sufficient to constrain ENSO simulations?, *Geophysical Research Letters*, *36*, L12,702, doi:10.1029/2009GL038710.
- Wittenberg, A. T. (2015), Low-frequency variations of ENSO, *US CLIVAR Variations*, *13*(1), 26–31.
- Wittenberg, A. T., A. Rosati, N.-C. Lau, and J. J. Ploshay (2006), GFDL’s CM2 global coupled climate models. Part III: Tropical Pacific climate and ENSO, *Journal of Climate*, *19*(5), 698–722, doi:10.1175/JCLI3631.1.

- Wittenberg, A. T., A. Rosati, T. L. Delworth, G. A. Vecchi, and F. Zeng (2014), ENSO modulation: Is it decadal predictability?, *Journal of Climate*, *27*(7), 2667–2681, doi:10.1175/JCLI-D-13-00577.1.
- Yoder, J. A., and M. A. Kennelly (2003), Seasonal and ENSO variability in global ocean phytoplankton chlorophyll derived from 4 years of seawifs measurements, *Global Biogeochemical Cycles*, *17*(4).
- Yu, J.-Y., and S. T. Kim (2010), Identification of central-Pacific and eastern-Pacific types of ENSO in CMIP3 models, *Geophysical Research Letters*, *37*(15).
- Zanchettin, D., M. Khodri, C. Timmreck, M. Toohey, A. Schmidt, E. P. Gerber, G. Hegerl, A. Robock, F. S. R. Pausata, W. T. Ball, S. E. Bauer, S. Bekki, S. S. Dhomse, A. N. LeGrande, G. W. Mann, L. Marshall, M. Mills, M. Marchand, U. Niemeier, V. Poulain, E. Rozanov, A. Rubino, A. Stenke, K. Tsigaridis, and F. Tummon (2016), The model intercomparison project on the climatic response to volcanic forcing (VolMIP): experimental design and forcing input data for CMIP6, *Geoscientific Model Development*, *9*(8), 2701–2719, doi:10.5194/gmd-9-2701-2016.
- Zavala-Garay, J., C. Zhang, A. M. Moore, A. T. Wittenberg, M. J. Harrison, A. Rosati, J. Vialard, and R. Kleeman (2008), Sensitivity of hybrid ENSO models to unresolved atmospheric variability, *J. Climate*, *21*, 3704–3721, doi:10.1175/2007JCLI1188.1.
- Zebiak, S. E., and M. A. Cane (1987), A model El Niño-Southern Oscillation, *Monthly Weather Review*, *115*(10), 2262–2278.
- Zheng, F., X.-H. Fang, J.-Y. Yu, and J. Zhu (2014), Asymmetry of the Bjerknes positive feedback between the two types of El Niño, *Geophysical Research Letters*, *41*(21), 7651–7657.

Table 1. Comparison of ENSO phase probabilities in the observational data and CM2.1 model output for neutral ENSO, Central Pacific El Niño, Eastern Pacific El Niño, and La Niña.

	Neutral ENSO	CP El Niño	EP El Niño	La Niña
Observations	0.43	0.23	0.11	0.23
CM2.1	0.49	0.16	0.08	0.27

Table 2. Summary of the experiments used in Sections 3.1-3.3 and 3.4.

Name	ENSO type	ENSO strength	Ensemble members	Pinatubo forcing coefficient	Forcing start month
Sections 3.1-3.3					
<i>NTE</i> CTR	Neutral	Neutral	10	0	-
<i>NTE</i> PRT			10	1	June
<i>CPE</i> CTR	Central Pacific	Moderate	10	0	-
<i>CPE</i> PRT	El Niño		10	1	June
<i>EPE</i> CTR	Eastern Pacific	Strong	10	0	-
<i>EPE</i> PRT	El Niño		10	1	June
<i>LAN</i> CTR	La Niña	Moderate	10	0	-
<i>LAN</i> PRT			10	1	June
Section 3.4					
<i>CTR</i> ₀	Eastern Pacific El Niño	Strong	1	0	-
<i>CTR</i> _α ^{<i>Feb</i>}			50	[0.001,...,0.05]	February
<i>PRT</i> _α ^{<i>Feb</i>}			50	[1.001,...,1.05]	February
<i>CTR</i> _α ^{<i>Jun</i>}			50	[0.001,...,0.05]	June
<i>PRT</i> _α ^{<i>Jun</i>}			50	[1.001,...,1.05]	June

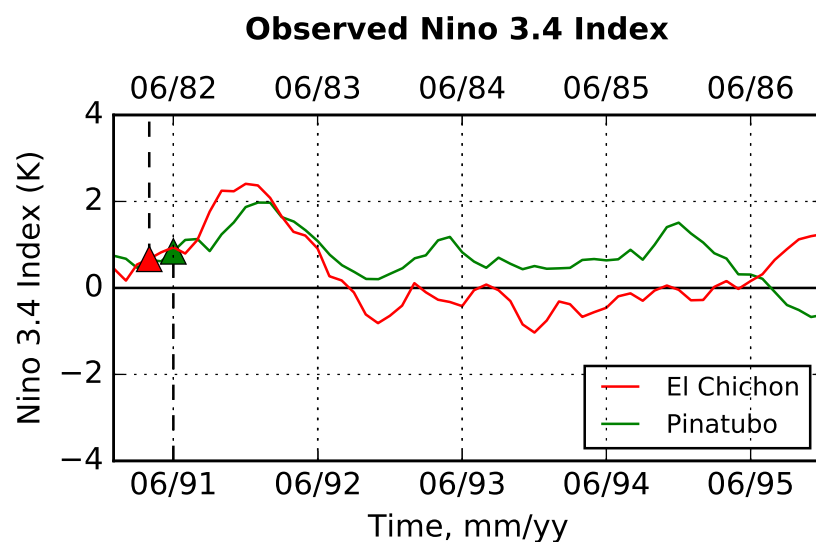


Figure 1. Observed Niño 3.4 index (K) evolution after the El Chichón (red, top x-axis) and Pinatubo (green, bottom x-axis) eruptions, calculated using the ERSST V4 dataset. Eruption dates are marked with triangles.

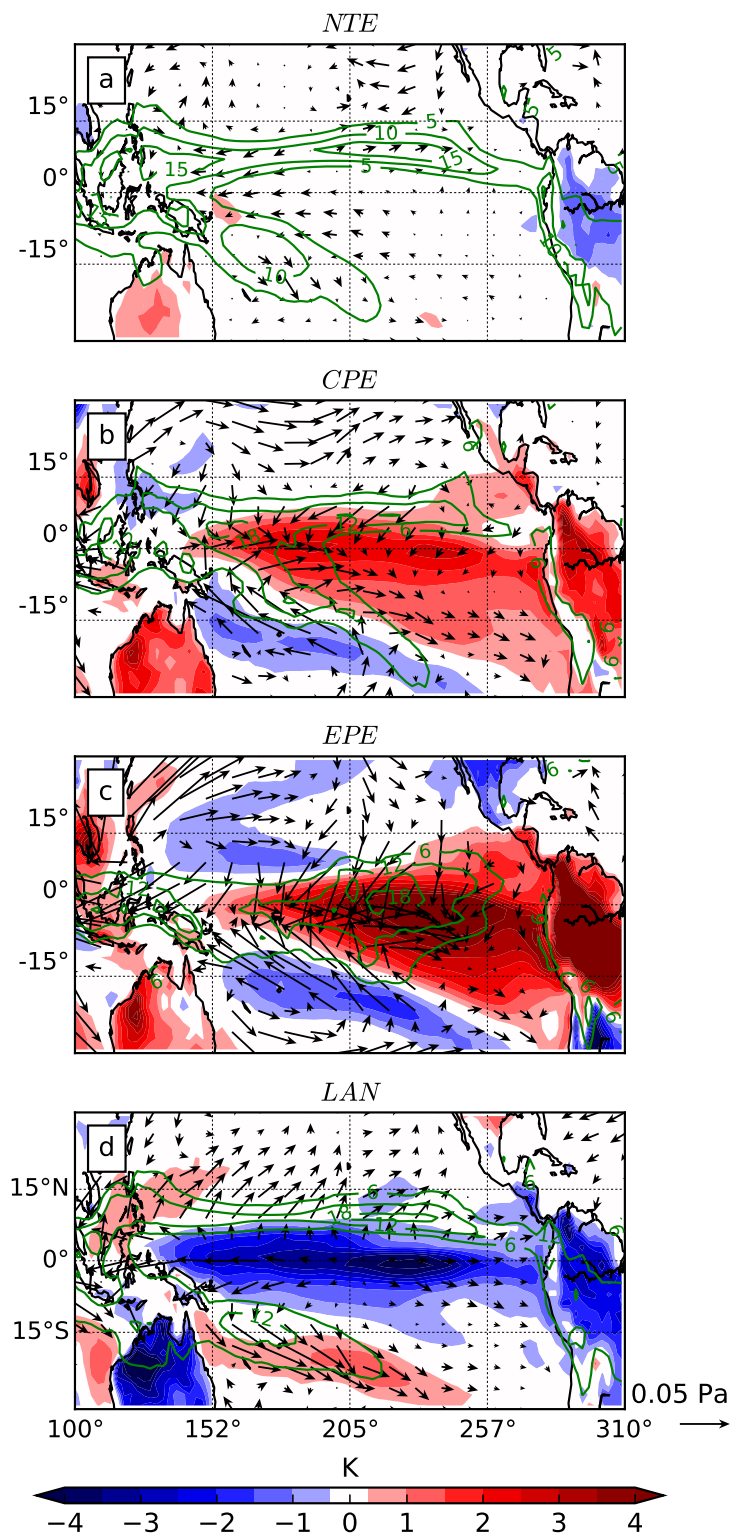


Figure 2. Simulated surface temperature (K, shading) and surface wind stress vector (Pa, arrows) anomalies with respect to the climatology (CTR-CLM), and total precipitation (mm day⁻¹, contours) of the 10-member control ensemble mean ENSO phases in December 1991: a) neutral ENSO (*NTE*), b) Central Pacific El Niño (*CPE*), c) Eastern Pacific El Niño (*EPE*), and d) La Niña (*LAN*).

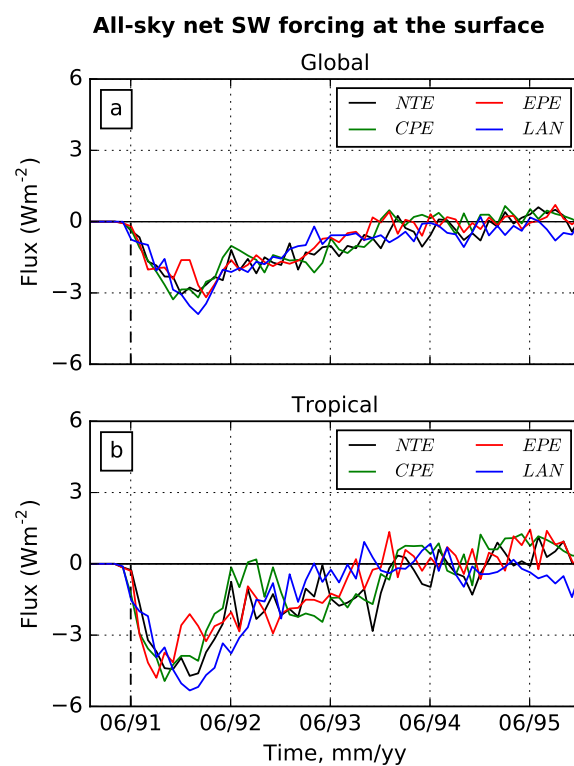


Figure 3. Simulated a) global and b) tropical (20°S-20°N) all-sky net (down-up) shortwave (SW) radiative forcing at the surface (W m^{-2}) calculated as a 10-member ensemble mean difference (PRT-CTR) for neutral ENSO (*NTE*, black), Central Pacific El Niño (*CPE*, green), Eastern Pacific El Niño (*EPE*, red), and La Niña (*LAN*, blue) experiments.

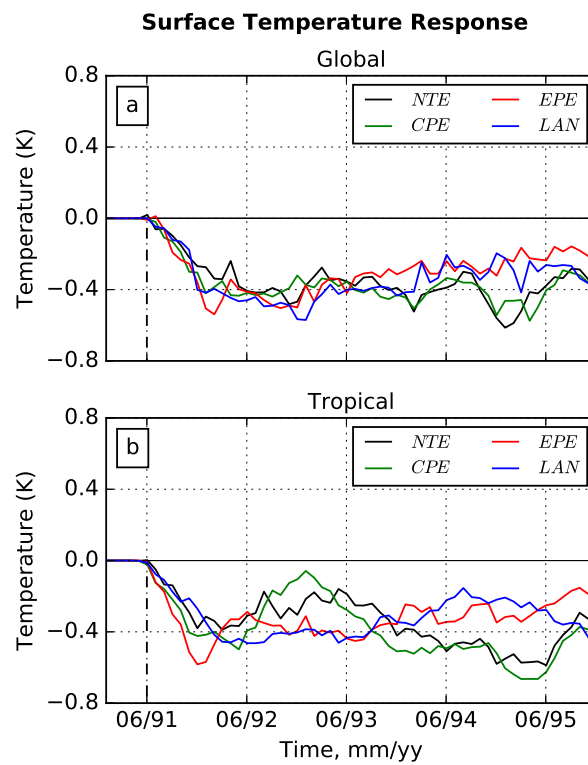


Figure 4. Same as in Figure 3 but for the surface temperature response (K).

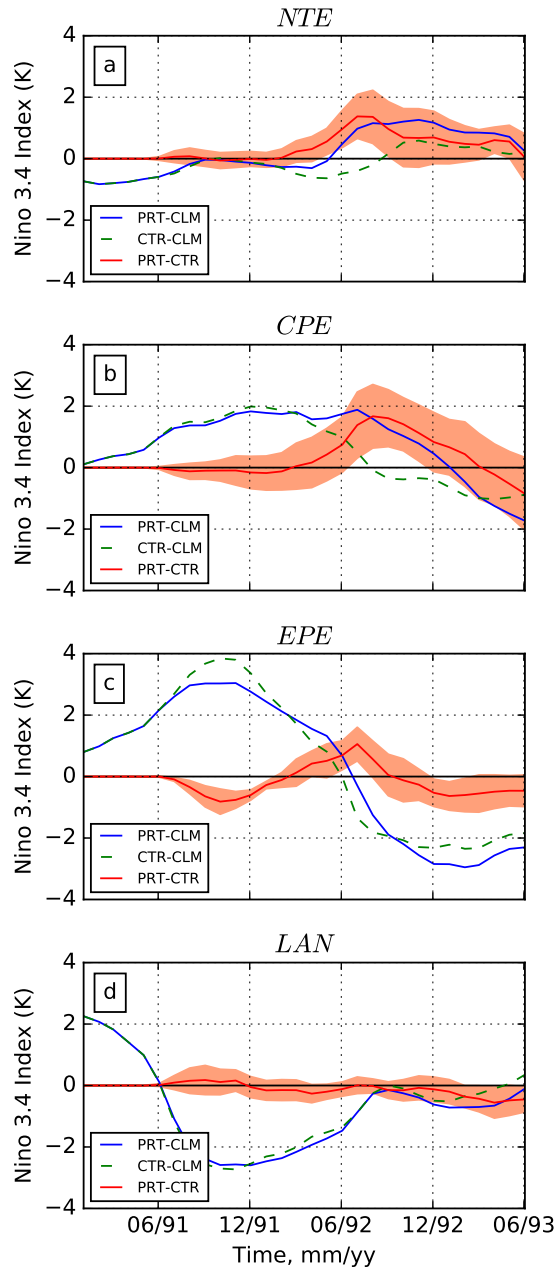


Figure 5. Simulated control (green dash) and perturbed (blue) Niño 3.4 index (K) calculated using 10-member ensemble means, and difference between them (PRT-CTR) (red) in the a) neutral ENSO (*NTE*), b) Central Pacific El Niño (*CPE*), c) Eastern Pacific El Niño (*EPE*), and d) La Niña (*LAN*) experiments. Red shading depicts 95% confidence intervals for the ensemble mean difference.

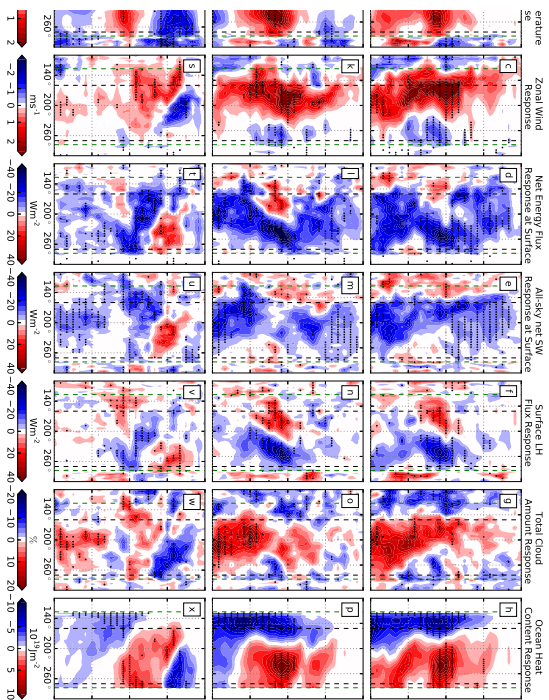


Figure 6. Hovmöller diagrams of simulated net (down-up) clear-sky shortwave (SW) surface flux (W m^{-2}), surface temperature (K), zonal wind (m s^{-1}), net surface heat flux, and all-sky net (down-up) shortwave (SW) fluxes at the surface, latent heat (LH) flux (W m^{-2}), total cloud amount (%) and top 300 m ocean heat content (10^{19} J m^{-2}) 10-member ensemble mean response (PRT-CTR) to a Pinatubo-size volcanic perturbation. Values are averaged over 5°S - 5°N for neutral ENSO (NTE, a-h), Central Pacific El Niño (CPE, i-p), and Eastern Pacific El Niño (EPE, q-x) experiments for June 1991-June 1993. Black dots define the statistical significance at the 0.05 level. Dashed black and green lines indicate the bounds of the Niño3 + Niño4 region and coastal boundaries of the equatorial Pacific ocean, respectively. Red and blue colors of wind correspond to westerly and easterly anomalies, respectively.

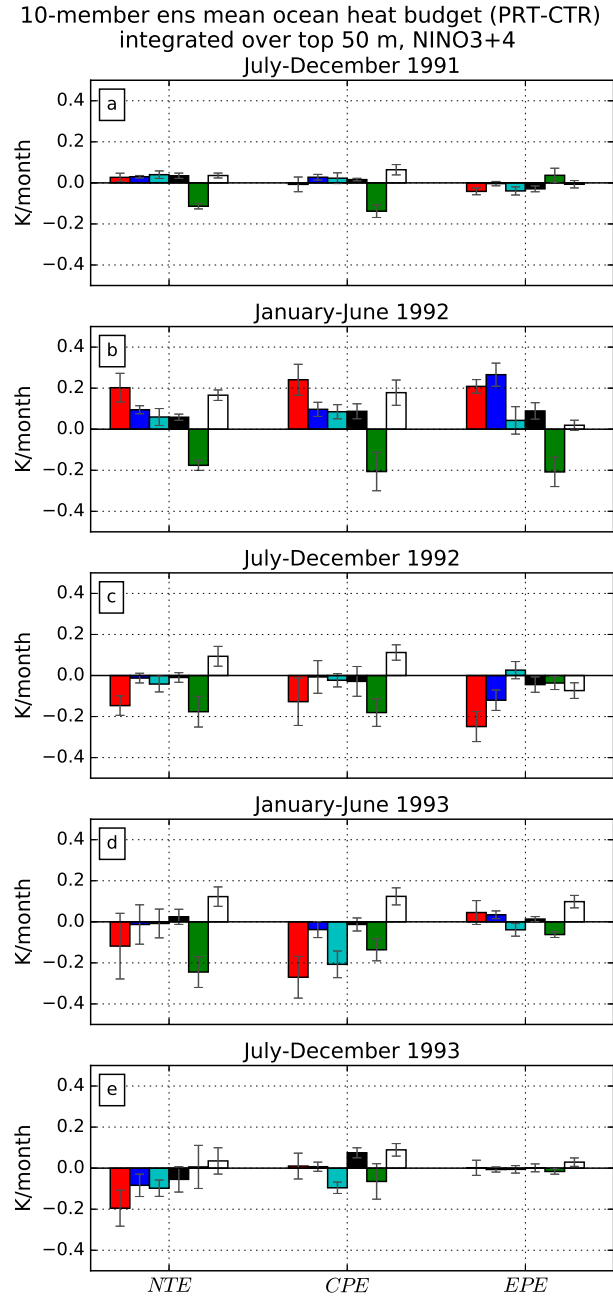


Figure 7. Simulated eruption response of the oceanic top 50 m total temperature tendency (K/month) (red), thermocline feedback and ocean dynamical thermostat (blue), zonal advection (cyan), meridional advection (black), net surface heat flux (green), and residual (white) for the time intervals: a) July-December 1991, b) January-June 1992, c) July-December 1992, d) January-June 1993, e) July-December 1993. Within each time interval, the 10-member ensemble mean *NTE*, *CPE*, and *EPE* responses to the Pinatubo eruption (PRT-CTR) are shown. The values are integrated over the narrowed Niño3 + Niño4 region (2°S-2°N, 160°E-90°W). Error bars show the standard error of the ensemble-mean difference, which increases with time as both ensembles chaotically disperse.

SST and wind stress, 10-member ensemble mean response

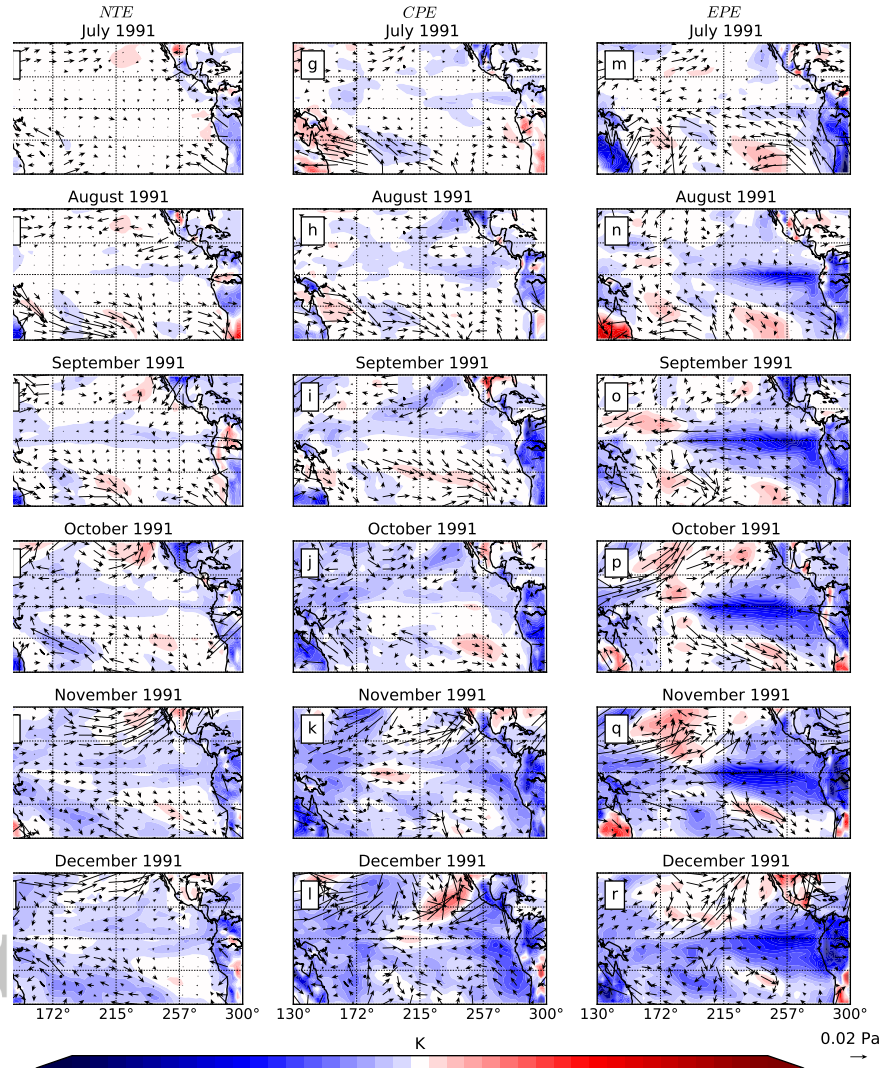


Figure 8. Simulated surface temperature (K, shading) and surface wind stress vector (Pa, arrows) 10-member ensemble mean response (PRT-CTR) to the Pinatubo radiative forcing in the neutral ENSO (NTE, a-f), Central Pacific El Niño (CPE, g-l), and Eastern Pacific El Niño (EPE, m-r) experiments for July-December 1991.

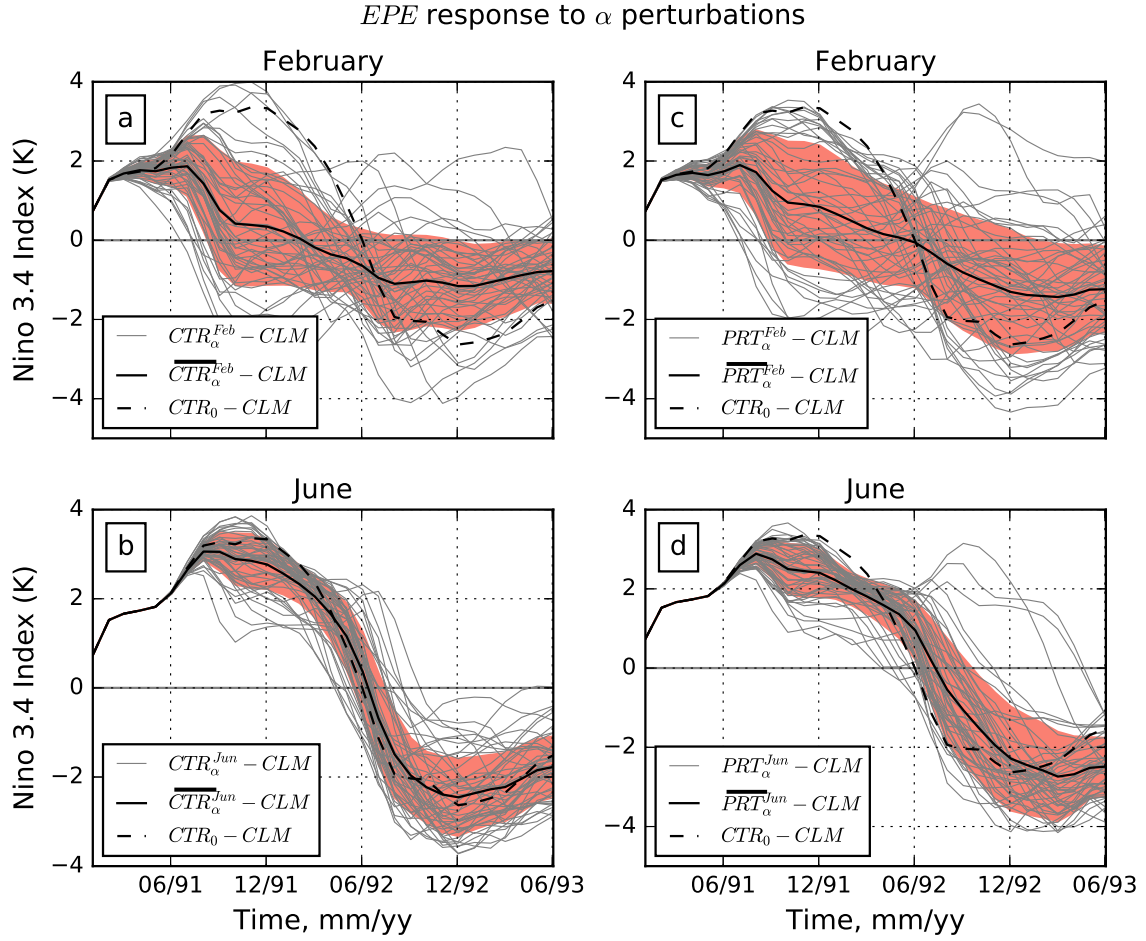


Figure 9. Comparison of simulated Niño 3.4 indexes (K) in a single reference Eastern Pacific El Niño realization (CTR_0) and 50-member control and perturbed ensembles with α perturbations in February (CTR_α^{Feb} , a; PRT_α^{Feb} , c) and June (CTR_α^{Jun} , b; PRT_α^{Jun} , d). Niño 3.4 indexes in single realizations (grey spaghetti curves), and ensemble means (black solid curve) are calculated with respect to the climatology. Bars denote the ensemble mean quantities. Red shading depicts $\pm\sigma$ ensemble variability.

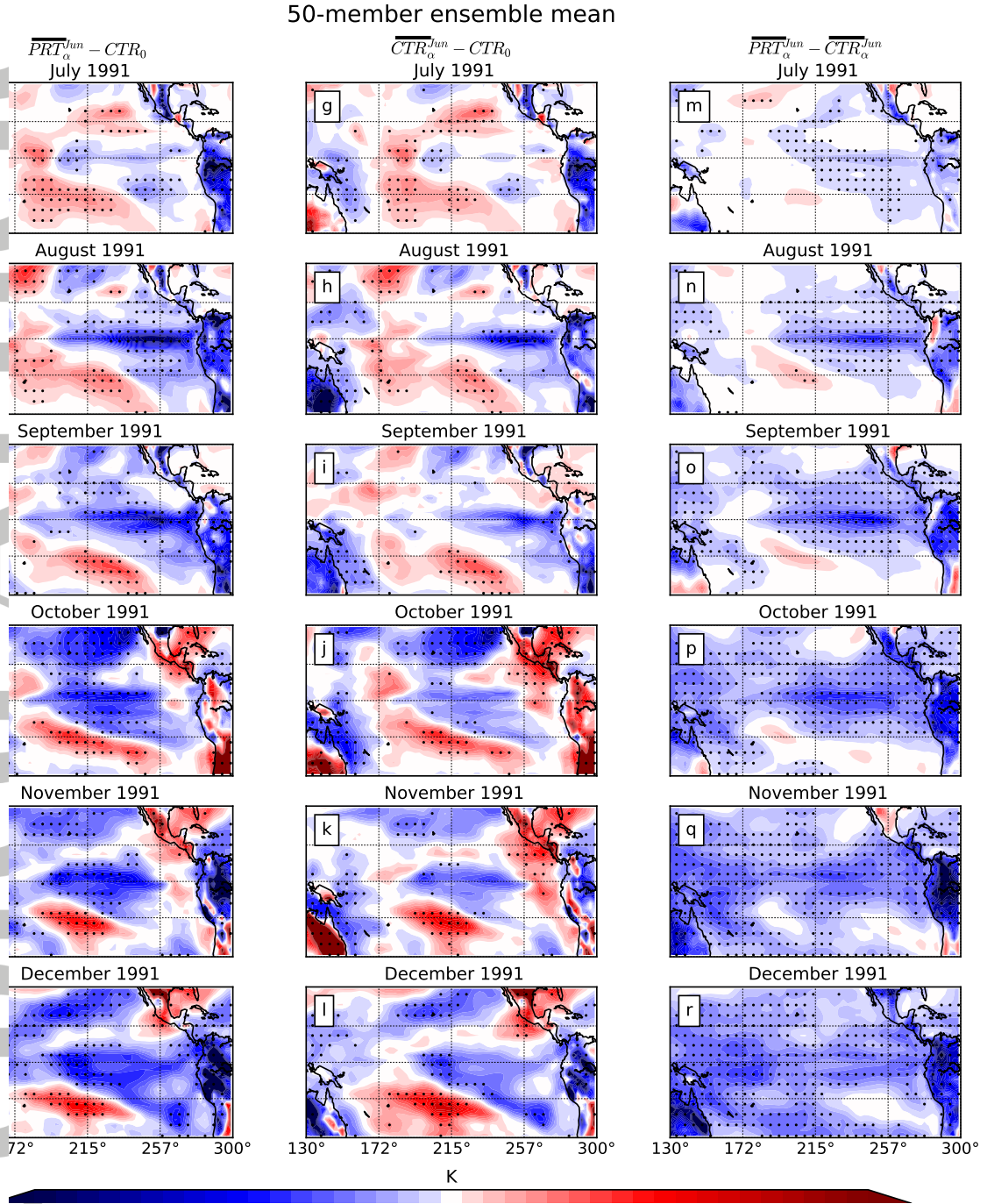


Figure 10. Simulated monthly averaged surface temperature (K, shading) 50-member perturbed (PRT_{α}^{Jun} , a-f) and control (CTR_{α}^{Jun} , g-l) ensemble means with α perturbations calculated as anomalies with respect to a single reference Eastern Pacific El Niño realization (CTR_0), and difference between PRT_{α}^{Jun} and CTR_{α}^{Jun} (m-r) for July-December 1991. Black dots indicate areas where the reference surface temperature is below the 10th percentile or above the 90th percentile for the 50-member CTR_{α}^{Jun} (a-f) and PRT_{α}^{Jun} (g-l) ensemble distributions, and statistical significance of the ensemble-mean surface temperature difference calculated using two-tailed Student's t-test at the 0.05 significance level (m-r).

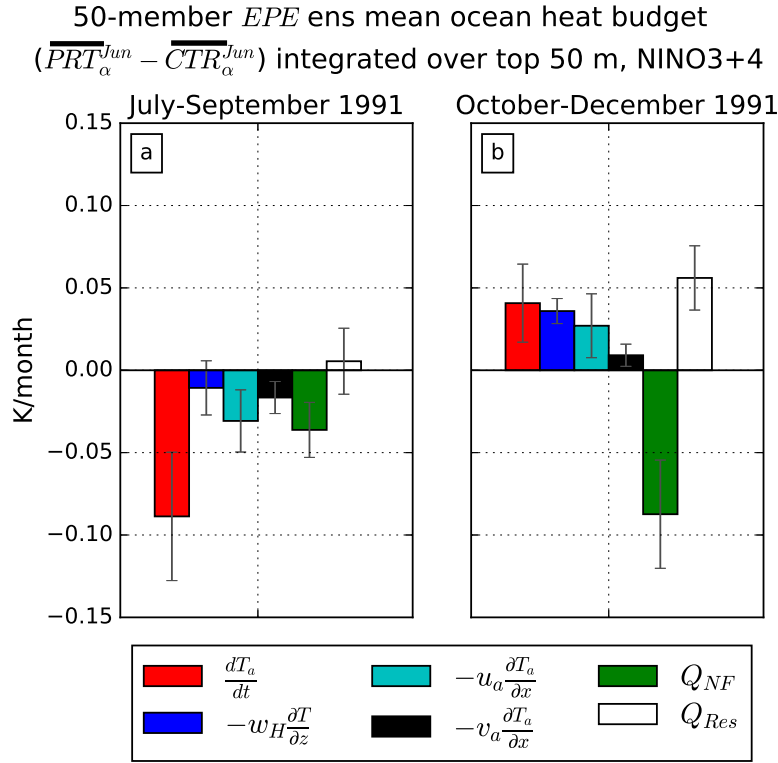


Figure 11. Simulated oceanic top 50 m total temperature tendency (K/month) (red), thermocline feedback (blue), zonal advection (cyan), meridional advection (black), net surface heat flux (green), and residual (white) for the time intervals: a) July-September 1991, b) October-December 1991. Within each time interval, the 50-member ensemble mean Eastern Pacific El Niño response to the Pinatubo eruption ($\overline{PRT}_\alpha^{Jun} - \overline{CTR}_\alpha^{Jun}$) is shown. The values are integrated over the narrowed Niño3 + Niño4 region (2°S-2°N, 160°E-90°W). Error bars show the standard error of the mean difference.